8

Minisini, Daniel, Patricio Desjardins, Germán Otharán, Maximiliano Paz, Diego Kietzmann, Gregor Eberli, Carlos Zavala, Toni Simo, James H. Macquaker, and Christian Heine, 2020, Sedimentology, depositional model, and implications for reservoir quality, *in* Daniel Minisini, Manuel Fantín, Iván Lanusse Noguera, and Héctor A. Leanza, eds., Integrated geology of unconventionals: The case of the Vaca Muerta play, Argentina: AAPG Memoir 121, p. 201–236.

Sedimentology, Depositional Model, and Implications for Reservoir Quality

Daniel Minisini and Patricio Desjardins

Shell Exploration and Production, 150 Dairy Ashford, Houston, Texas 77079 (e-mails: daniel.minisini@shell.com; p.desjardins@shell.com)

Germán Otharán

Departamento de Geología, Universidad Nacional del Sur, Bahía Blanca 8000, Argentina; GCS Argentina SRL. Florencio Molina Campos 150, Bahía Blanca 8000, Argentina (e-mail: german.otharan@uns.edu.ar)

Maximiliano Paz

University of Saskatchewan, 6982 Saskatchewan, Canada (e-mail: maxi.paz@usask.ca)

Diego Kietzmann

IGeBA, Consejo Nacional de Investigaciones Científicas y Técnicas, Departamento de Ciencias Geológicas, Facultad de Ciencias Exactas y Naturales, Universidad de Buenos Aires, Ciudad Universitaria, Pabellón II, Intendente Güiraldes 2160, C1428EHA Buenos Aires, Argentina (e-mail: diegokietzmann@gl.fcen.uba.ar)

Gregor Eberli

Center for Carbonate Research, University of Miami, 4600 Rickenbacker Causeway, Miami, Florida 33149 (e-mail: geberli@rsmas.miami.edu)

Carlos Zavala

Departamento de Geología, Universidad Nacional del Sur, Bahía Blanca 8000, Argentina; GCS Argentina SRL. Florencio Molina Campos 150, Bahía Blanca, 8000, Argentina (e-mail: czavala@gcsargentina.com)

Toni Simo and James H. Macquaker

ExxonMobil, 22777 Springwoods Village Parkway, Spring, Texas 77389 (e-mails: toni.t.simo@exxonmobil.com; james.h.macquaker@exxonmobil.com)

Christian Heine

Shell Global Solutions International B.V., Lange Kleiweg 40, 2288 GS Rijswijk, The Netherlands (e-mail: christian.heine@shell.com)

ABSTRACT

This contribution integrates lithologic, mineralogical, geochemical, and geomechanical data from cores and outcrops, and emphasizes where and how sedimentology may help the exploration of self-sourced unconventional reservoirs. In fact, the activity in the unconventional

DOI: 10.1306/13682228M1203264

plays has boosted the research on the sedimentology of mudstones to better define the sweet spots and the landing zones sought by industry. This chapter describes the stratigraphic architecture of the Vaca Muerta-Quintuco system (prograding clinoforms ~150 km long and 300 m high), the lithology per sector (e.g., carbonate in the topsets, marlstone in the foresets, mudstone in the bottomsets), and reconstruct genetically-related facies defining a depositional model where sediment arrives from topset and currents move it basinward into a suboxic environment of deposition. The stratigraphic framework created is then populated with rock characteristics to create a play concept and define sweet spots and landing zones.

INTRODUCTION

The understanding of sedimentological controls on reservoir quality enables not only a detailed reservoir characterization but also an interpretation of the evolution of sedimentary environments, which are useful to predict the variation of the facies and their associated reservoir properties. Facies with potential high–bulk-volume hydrocarbons and prone to fracture define the best areas to land horizontal wells. Therefore, the analyses of cores and outcrops become fundamental for the geologic understanding and calibration to the subsurface because their lithological fabric defines the type and quantity of pores that, in turn, define the amount of hydrocarbon residing within. Furthermore, the descriptions of cores and outcrops address the vertical facies heterogeneity that plays a key role in hydraulic fracture height. Although subject to weathering, outcrops allow pseudo three-dimensional visualization of the sedimentary features showing the lateral variability of the facies, which is important to infer the depositional processes, to analyze the stratigraphic terminations of the beds, and to explain the role played by structural elements. The cores, undisturbed by weathering, provide key information about rock mineralogy, texture, porosity, saturation, and organic content directly applicable to petrophysical and geomechanical models that determine in-place volume (Figure 1).

During the past decade, the sedimentology of fine-grained deposits has received greater attention because of the growing interest in self-sourced unconventional reservoirs (e.g., Eagle Ford, Haynesville, Marcellus, Utica, Barnett, and Bakken), leading to detailed analyses on a variety of organic-rich mudstones, the most representative lithology of these reservoirs. Additionally, laboratory research (e.g., Schieber et al., 2007, 2013; Schieber and Southard, 2009; Schieber and Yawar, 2009; Yawar and Schieber, 2017) and investigations of modern systems (e.g., Baudin et al., 2010, 2017a, b; Biscara et al., 2011; Stetten et al., 2015; Mignard et al., 2017; Tesi et al., 2017) have provided novel information on the mechanisms that control mud distribution, contributing to a gradual paradigm shift in mudstone sedimentology (Soyinka and Slatt, 2008; Bhattacharya and MacEachern, 2009; Macquaker et al., 2010; Schieber et al., 2010; Plint et al., 2012; Schieber and Bennett, 2013; Bohacs et al., 2014; Könitzer et al., 2014; Wilson and Schieber, 2014, 2015; Lazar et al., 2015; Schieber, 2016; Zavala and Arcuri, 2016). The accumulation of organic-rich mudstones was historically associated with fallout from dilute buoyant plumes, low-energy depositional environments, and anoxic bottom waters (e.g., Pettijohn, 1975; O'Brien and Slatt, 1990; Boggs, 2001; Potter et al., 2005). Now, research has revealed that bottom-water anoxia is not necessarily a prerequisite for the preservation of organic matter and that the role of fallout processes is probably subordinate to the occurrence of punctuated bottom currents (e.g., Macquaker and Gawthorpe, 1993; Wilson and Schieber, 2014; Lash, 2016; Minisini et al., 2018).

In Argentina, the early Tithonian–early Valanginian Vaca Muerta Formation is composed of organic-rich calcareous mudstone representing South America's main self-sourced unconventional play since 2010 (see Minisini et al., 2020, this Memoir). The new cores recovered in the subsurface and the widespread excellent outcrops along the thrust-and-fold belt, just a few tens of kilometers west of the Vaca Muerta play, provide a great opportunity for an integrated study of the depositional history of the Vaca Muerta Formation in a bed-to-basin scale. Before the renewed interest on mudstones as reservoirs, this formation was studied for its paleontological richness and world-class source rock and was described and interpreted as monotonous mudstones accumulated by fallout in quiet and anoxic deep marine environments (Leanza et al., 1977; Legarreta et al., 1981; Mitchum and Uliana, 1985; Legarreta and Uliana, 1991). However, recent sedimentological research and reservoir characterization (e.g., Kietzmann et al., 2011, 2014; Galeazzi et al., 2014; González et al., 2018) have documented that the Vaca Muerta Formation is a highly heterogeneous unit whose depositional processes are certainly more variable, as noted when describing the rocks at decimeter-to-millimeter scale (Zeller et al., 2015a, b; Otharan et al., 2018, 2020; Paz et al., 2019). The chapter summarizes this recent research integrating new data and interpretations to offer explorers an analog to help define sweet spots and landing zones in other unconventional plays.

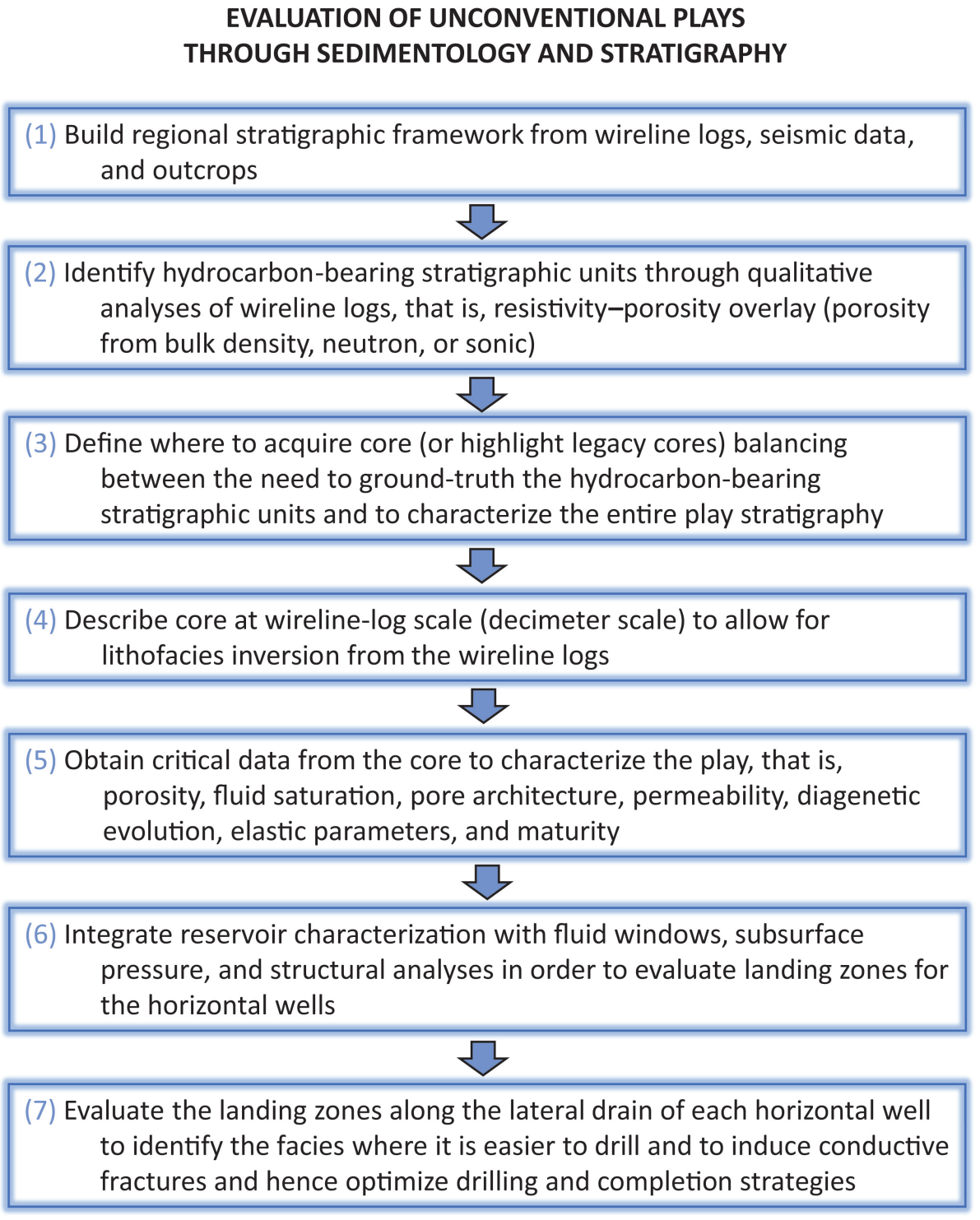

Figure 1. Workflow outlining the procedures that emphasize the importance of sedimentology and stratigraphy in the evaluation of new unconventional plays and in the optimization of long-term productive plays.

GEOLOGICAL SETTING

During early Tithonian to early Valanginian, the Neuquén Basin was an embayment bounded to the west by a volcanic island arc with narrow marine passages, to the east by a shallow shelf, to the south by the North Patagonian Massif (see Domínguez et al., 2020b, this Memoir), whose tectonic reactivations and humid climatic conditions (Huincul and Chihuidos highs) triggered frequent and intense siliciclastic input (e.g., Orchuela et al., 1981; Legarreta and Uliana, 1991), and to the north by the arid area of the Mendoza embayment. This configuration allowed the coexistence of shallow-marine carbonate ramps and mixed carbonate–siliciclastic clinoforms around the basin margins. The Vaca Muerta Formation corresponds to the distal facies of a marine shallowing-upward sedimentary cycle of second order (*sensu* Vail et al., 1977), known as the Vaca Muerta–Quintuco system (Spalletti and Veiga, 2007). The large seismic data set created by the oil and gas (O&G) Industry displays this system as a clear set of multiple clinoforms (see Domínguez et al., 2020a, this Memoir) and is shown here as subdivided into six units named *sensu* Desjardins et al. (2018) (figure 2 and figure 5 of Minisini et al., 2020, this Memoir). This chapter associates the Vaca Muerta Formation to the bottomsets and foresets of the clinoforms, consisting of mudstones and marlstones interbedded with limestones and extremely thin volcaniclastic layers (aka bentonites, tuffs, and tephras). The Quintuco Formation (not treated in this chapter) is associated to the topsets, consisting of bindstones, grainstones, wackestones, and dolostones (Kietzmann et al., 2020, this Memoir).

The clinoforms are formed by the transgressive-regressive cycles of the sea level. In general, transgressive hemi-cycles are characterized by more organic and siliciclastic content and less carbonate, vice versa for the regressive hemi-cycles (Kietzmann et al., 2016; Eberli et al., 2017; see figure 18 in Reijenstein et al., 2020, this Memoir). The progradational clinoforms migrated toward northwest and created a basinwide vertical stack of organic-rich units, typically preserved in the bottomsets and lower foresets (Figure 3). It is in this vertical stack of organic-rich units that the O&G Industry is landing the unconventional horizontal wells (see Vittore et al., 2020, this Memoir; Notta et al., 2020, this Memoir; Nielsen et al., 2020, this Memoir; Estrada et al., 2020, this Memoir).

In the Jurassic clinoforms (Units 1 to 3), the storm-wave base level interface, at around 50 to 70 m (160 to 230 ft) of paleo water depth (Kietzmann and Palma, 2011), did not produce a substantial change in the proportions nor in the stacking patterns of the lithofacies,

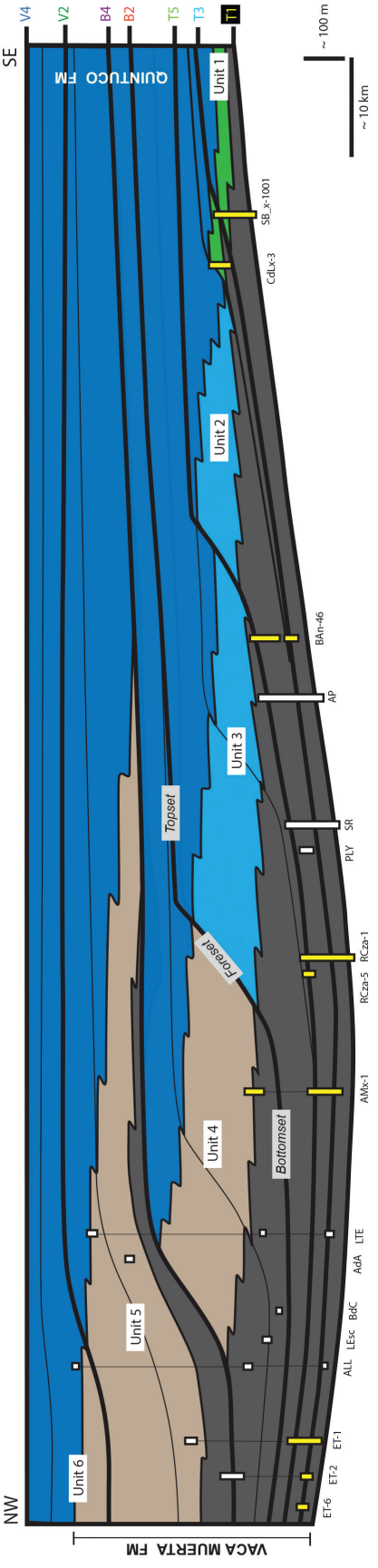

Figure 2. Simplified stratigraphic architecture of the Vaca Muerta–Quintuco system, based on seismic features and wells (location in Figure 3). Quintuco Formation is associated with Motif E (dark blue). Note that the contact between Vaca Muerta and Quintuco formations is diachronous. Units and surfaces follow the "Rosetta Stone" in figure 5 of Minisini et al., 2020, this Memoir.

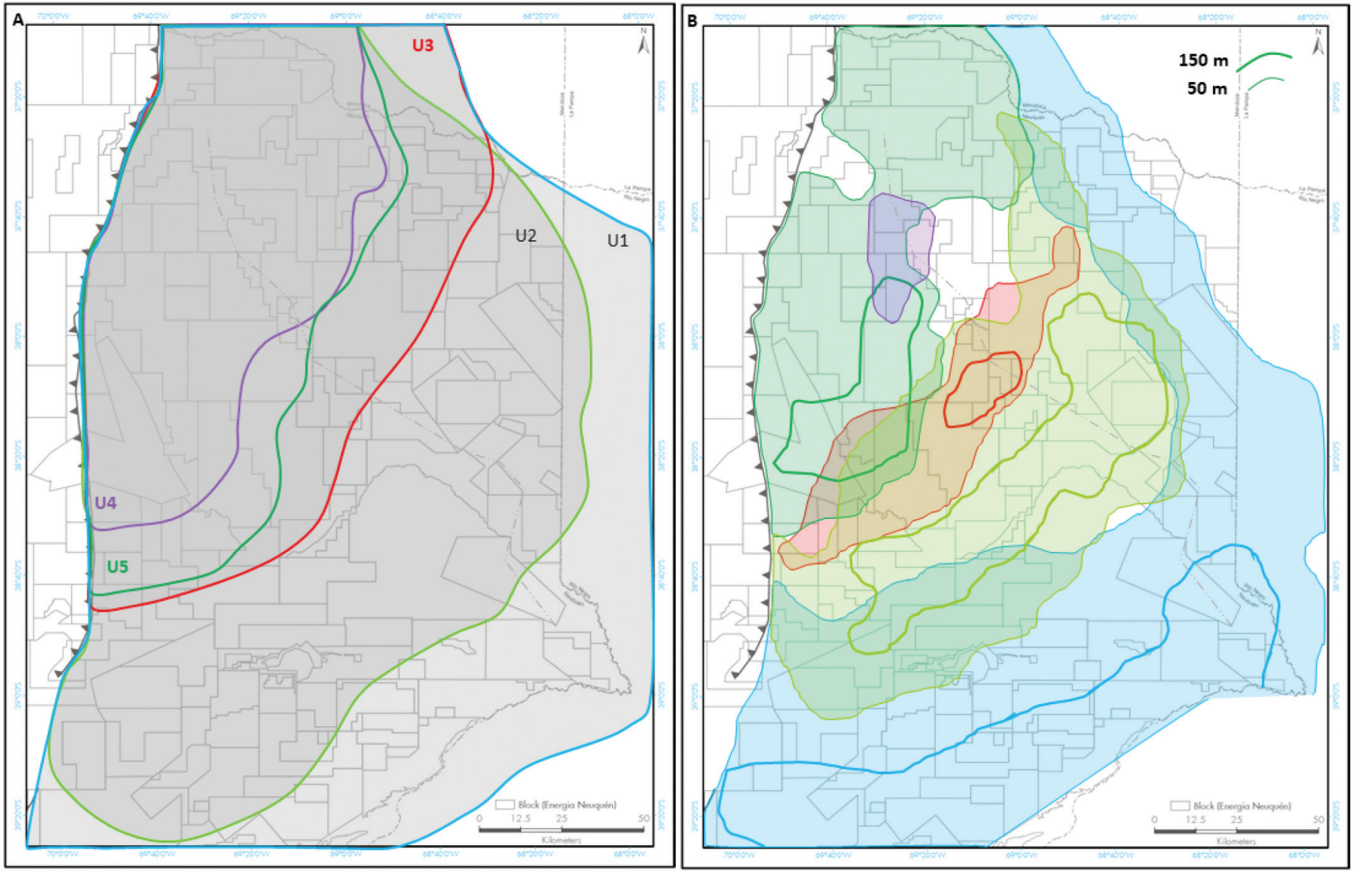

Figure 3. (A) Extent of the organic-rich sections in the Vaca Muerta–Quintuco system (TOC > 2%) (see stratigraphic units in Figure 2). The organic-rich sections occur in the bottomsets and lower foresets, which are the best depositional sectors to land the horizontal wells. (B) Thickness of the organic-rich sections indicated by 50 and 150 m [~160 and 500 ft] contours. Most data are derived from Domínguez et al., 2018. Dashed gray line is the cross section in Figure 2. TOC = total organic carbon.

suggesting low-energy environments with moderate storms. In contrast, in the Cretaceous clinoforms (Units 4 to 6), the significantly higher input of siliciclastic material determined a clear shelf break, increased the foresets angle from less than 1° to 2°–3°, and created a substantial heterogeneity in the lithofacies (Mitchum and Uliana, 1985; Zeller et al., 2015a; Kietzmann et al., 2016).

METHODS

To analyze the reservoir heterogeneity in the Vaca Muerta play, sedimentological studies were carried out from tens of cores in different positions of the Neuquén Basin (not presented in this work) (Figure 2). In this chapter, two representative cores (SB x-1001 in the Sierras Blancas block and AM x-1 in the Aguila Mora block) allowed the recognition of 12 lithofacies (LF) described in terms of texture, mineralogy, sedimentary structures, allochem types, diagenesis, and bioturbation (Figures 4, 5, Table 1).

The changes in mineralogy and texture are specifically highlighted, as their interplay controls two key aspects for the hydrocarbon production: the reservoir properties (e.g., porosity, oil saturation) and the geomechanical properties (e.g., rock stiffness, stress).

Routine analyses made on the cores include petrography (thin sections, scanning electron microscopy [SEM] images), geochemistry (total organic carbon [TOC], spectral gamma ray [SGR], and x-ray diffraction [XRD]) and geomechanics (shale rock properties, Young's modulus, and Poisson's ratio). Lithofacies were defined at bedset scale (decimeter scale) to tie them to the well log curves, but specific units were described at millimeter scale to decipher their depositional processes. After the well-to-seismic tie, the lithofacies were projected to seismic sections to integrate the basinwide sequence stratigraphic framework (see Domínguez et al., 2020a, this Memoir). The results of this integrated sedimentological study can be used to (1) link lithofacies to reservoir quality; (2) predict lateral variations of reservoir properties; (3) evaluate the number of potential landing zones; and (4) highlight potential frack barriers and baffles (Figure 1).

DEPOSITIONAL MOTIFS

Most of the 12 lithofacies identified (Figure 5, Table 1) record low-energy depositional processes; nevertheless some facies are related to bottom currents (LF 3 and 5), and gravity flows (LF 7 and 9) suggesting more

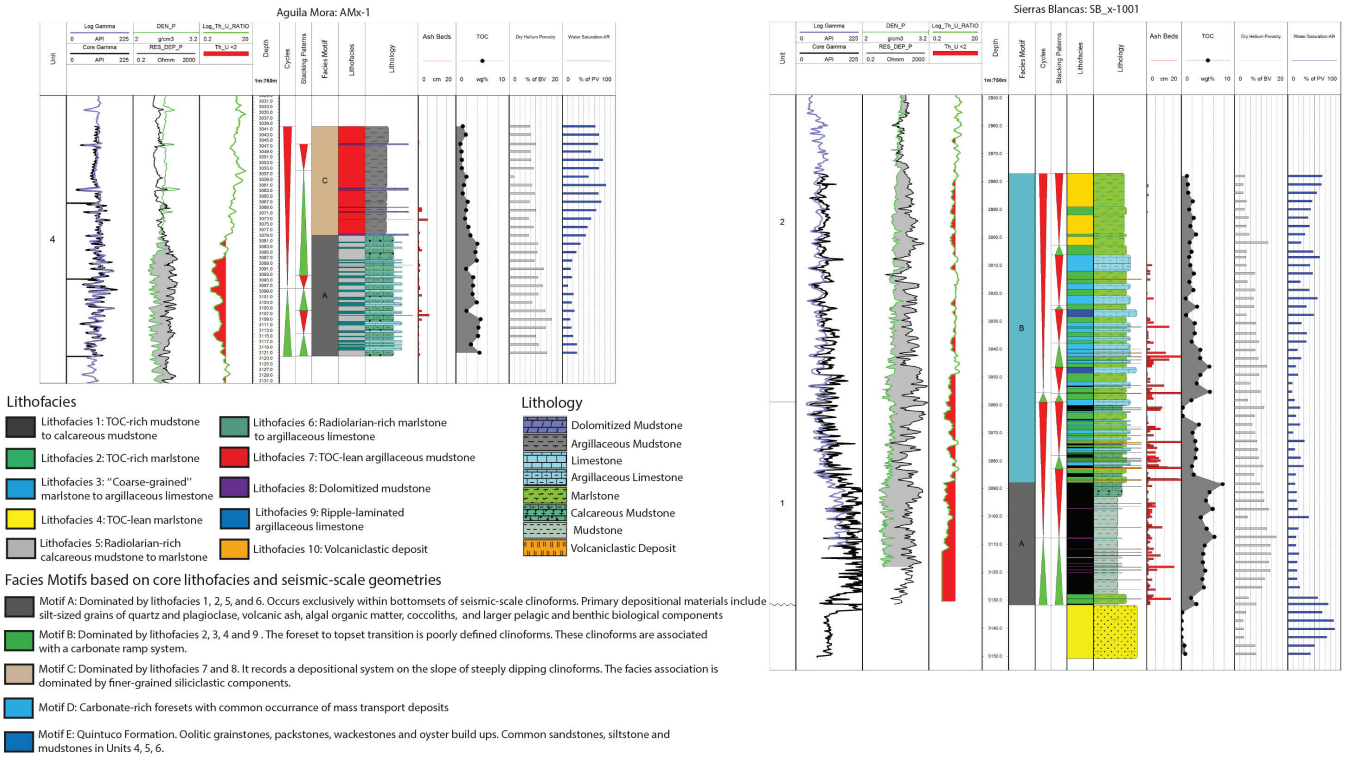

Figure 4. Cores and logs showing the type and intensity of vertical heterogeneity in the reservoir facies (see stratigraphic location in Figure 2).

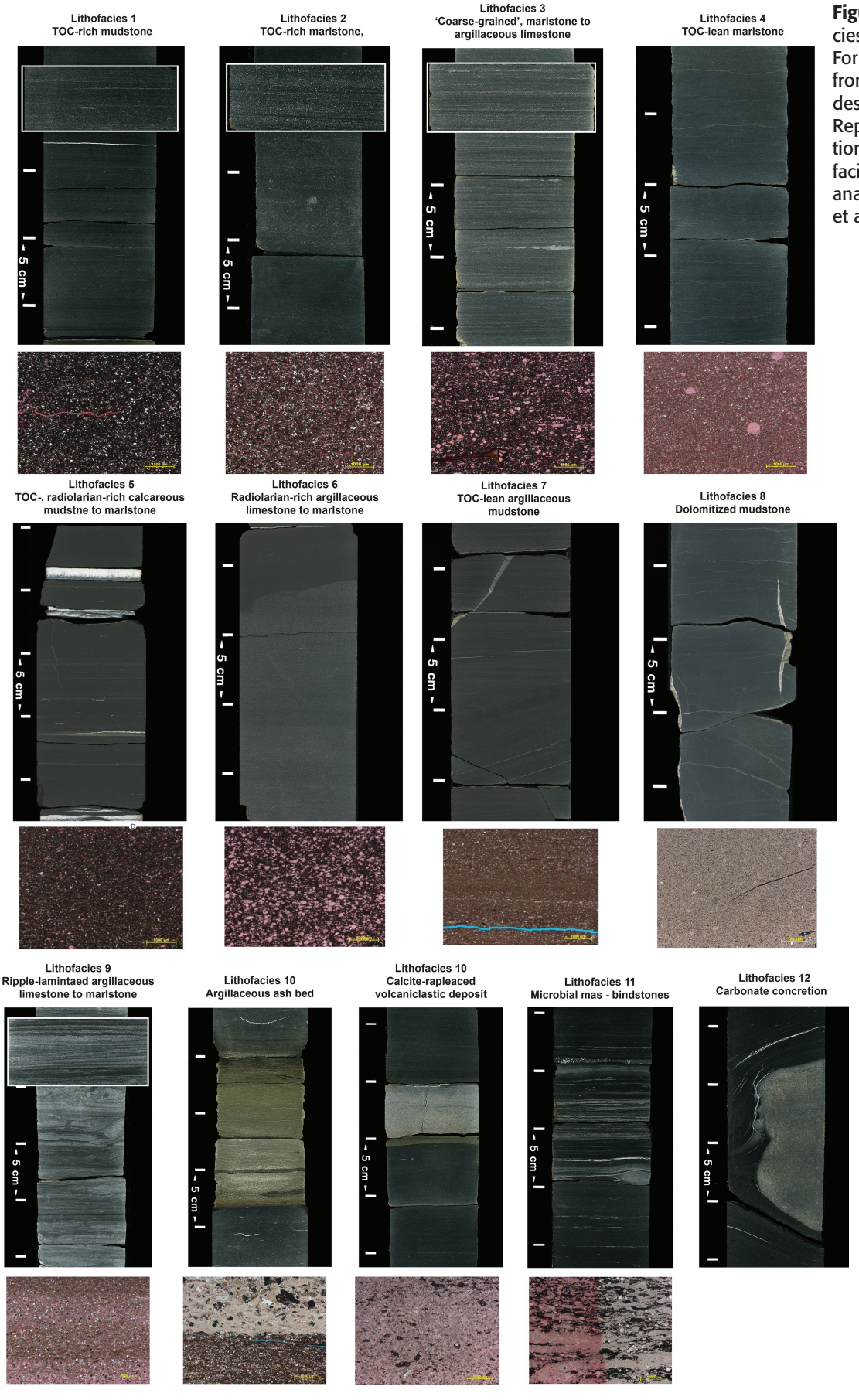

Figure 5. Main lithofacies of the Vaca Muerta Formation as identified from core analyses (full description in Table 1). Representative thin sections are below the lithofacies (see thin sections analyses in Kietzmann et al., 2020, this Memoir).

Table 1. Lithofacies of the Vaca Muerta Formation identified from core analyses. Last column from Kietzmann et al., 2020, this Memoir.

Lithofacies	Name	Description	Processes	Sedimentary Environment	Motif	Lithofacies in thin section
1	TOC-rich mudstone to calcareous mudstone	Massive to planar parallel-laminated, weakly to moderately bioturbated, organic-rich, mudstone to calcareous mudstone. Mix of light- (bioturbated) and dark-colored clay. Abundant fine sand to silt-size quartz and plagioclase grains. Abundant organic matter and phosphatic fragments, partially replaced by pyrite and dispersed altered volcanic ash. Common, locally very abundant, bivalve and ammonite molds and casts. Locally, abundant pellets intraclasts. Scarce calcified radiolarians.	Pelagic and hemipelagic deposition and/or bedload deposition by pulses of weak bottom current	Bottomset to lower foreset (basin to outer ramp)	A	Organic-rich mudstone ($_{OR}$Fl, $_{OR}$Fm), mudstones with lenticular laminae (F_{pi}ll)
2	TOC-rich marlstone	Discontinuous planar parallel-laminated, weakly to moderately bioturbated, organic rich, marlstone. Abundant silt-size calcareous grains, quartz and plagioclase, and dispersed altered volcanic ash. Abundant bivalves, saccocomids, and calcified radiolarians. Common pellets and skeletal fragments.	Pelagic and hemipelagic deposition and/or fallout of resuspended sediments by storms	Bottomset to lower foreset (basin to outer ramp)	A; B	Bioclastic wackestones/packstones (WP_bh, WP_bm, WP_oh, W_{sp}h, WP_sh)
3	"Coarse-grained" marlstone to argillaceous limestone	Discontinuous planar to continuous low-angle parallel-laminated, commonly strongly bioturbated, coarse-grained marlstone to argillaceous limestone. Common truncations and graded beds. Abundant silt-size skeletal fragments and fine sand-size pellets. Detrital carbonate in matrix. Common calcified radiolarians and bivalves. Locally abundant larger shell fragments in laminations. Scarce silt-size terrigenous grains.	Bedload transport by pulses of bottom currents	Foreset (outer to middle ramp)	B	Intraclastic packstone/grainstone (PG_ih), Peloidal packstones/grainstones (PG_ph)
4	TOC-lean marlstone	Massive to locally planar parallel-laminated, strongly bioturbated marlstone. Relatively low organic matter content. Abundant detrital carbonate in matrix, varying amount of skeletal fragments. Scarce silt-size terrigenous grains.	Pelagic and hemipelagic deposition and/or fallout of resuspended sediments by storms	Foreset (middle ramp)	B	Epistominid wackestone (W_eh)
5	Radiolarian-rich calcareous mudstone to marlstone	Massive to discontinuous parallel-laminated, organic-rich, calcareous mudstone to marlstone. Common calcified radiolarians, silt-size plagioclase grains, and coccolith pellets. Locally abundant Fe–dolomite silt, echinoderm fragments, ammonites, bivalves, and phosphatic fragments. Scarce intraclasts. Microcrystalline quartz in matrix.	Hemipelagic deposition and/or bedload deposition by pulses of weak bottom current. Intense diagenesis, radiolarians, and plagioclase replaced by calcite	Bottomset to lower foreset (basin to outer ramp)	A	Radiolaritic wackestones (W_rh)

Table 1. (*Continued*)

Lithofacies	Name	Description	Processes	Sedimentary Environment	Motif	Lithofacies in thin section
6	Radiolarian-rich marlstone to argillaceous limestone	Massive to discontinuous parallel-laminated, organic-rich, marlstone to argillaceous limestone. Truncations, graded beds, and lags are common. Very abundant calcified radiolarians and plagioclase grains, and coccoliths pellets. Microcrystalline quartz in matrix.	Fallout of resuspended sediments by storms and/or sediment gravity flows. Intense diagenesis, radiolarians, and plagioclase replaced by calcite	Bottomset to lower foreset (basin to outer ramp)	A	Radiolaritic wackestones (W_rh)
7	TOC-lean argillaceous mudstone	Parallel planar-laminated argillaceous mudstone. Common silt-size terrigenous grains (quartz and plagioclase), and silt-size Fe–dolomite grains. Lamination composed of alternating light-colored darker-colored laminae. Scarce calcified-replaced radiolarians. Common soft sediment deformation structures.	Sediment gravity flows and/or pulses of bottom currents. Mass transport movements in the slope	Foreset (middle ramp)	C	Organic-lean mudstone ($_{OL}$Fl)
8	Dolomitized mudstone	Dolostone, recrystallized, and few bivalve fragments and undifferentiated skeletal fragments. Scarce pellets, medium-colored clay between the dolomite crystals.	Early diagenesis associated with periods of low sediment accumulation rates.	Foreset (middle ramp)	C	Dolomitized mudstones (F_D), Dolostones (D)
9	Ripple-laminated marlstone to argillaceous limestone	Ripple-laminated to strongly bioturbated marlstone to argillaceous limestone. Alternations of calcareous-rich and calcareous-poor laminae. Abundant silt-size calcareous grains, quartz, plagioclase, and mudstone intraclasts. Common sponge fragments, echinoderms, forams, and calcified radiolarians. Common light-colored clay and dolomite.	Bedload and suspension fallout deposition by bottom currents and/or bottom currents	Foreset (middle ramp)	B	Heterolithic marlstone to limestone (Mrht, *PG*ht)
10	Volcaniclastic deposit	Massive to parallel-laminated, locally normally-graded, commonly bioturbated, volcaniclastic deposit composed of lithics fragments, plagioclase, size to silt pumiceous particles. Common calcite replacement or alteration to clay minerals of pumiceous and volcaniclastic lithics. Common disperse pyrite.	Ash fall and/or low-density turbidity flows. Calcite or clay replacement during early diagenesis	Bottomset to foreset (basin to middle ramp)	A; B	Lapillite (Lm, Lg), Calcite-replaced tuff (T_ch, T_cm), Clay-altered tuff (T_ah, T_am)
11	Microbial mats—bindstones	Alternation of parallel to subparallel wrinkle calcite and fine-grained marlstone	Microbial activity during periods of very low sedimentation rate and temporary anoxic conditions	Bottomset to lower foreset (basin to outer ramp)	A	Microbial bindstones (B_ml)
12	Carbonate concretion	Calcite nodules commonly encased in organic-rich mudstone, nucleated around ammonites, bivalve shells, or microfossils	Early diagenesis during periods of pause in sedimentation	Bottomset to lower foreset (basin to outer ramp)	A; B	Concretions (C)

energetic depositional conditions. In addition, lithofacies related to diagenetic processes (LF 8 and 12) and volcaniclastic fallouts (LF 10) are recorded, too (Table 1). The lithofacies distribution is not homogeneous along the clinoform. In fact, after the well-to-seismic tie, it becomes evident that some lithofacies commonly reoccur within the same depositional sector (i.e., bottomset, foreset, topset), hence generating lithofacies motifs described here (focus is on motifs with good reservoir characteristics: A, B, and C; see Figure 4).

Motif A (LF 1, 2, 5, 6, 10, 11, 12)

Motif A occurs in the bottomsets of clinoforms and is present in all sequences of the Vaca Muerta Formation (Figures 4, 5). It is characterized by an alternation of siliciclastic and calcareous mudstones rich in algal organic matter and includes silt-size quartz and plagioclase grains, volcanic fragments, coccoliths (delivered to the seafloor as fecal pellets), and biological components, mainly pelagic and less commonly benthic (i.e., radiolarians, ammonites, inoceramids, benthic foraminifera). Marlstones, bindstones, calcareous concretions, and argillaceous and calcified ash beds are also common constituents. Motif A is interpreted as the sedimentary record of distal bottomset to distal foreset (basin to outer ramp) deposited below the storm-wave base, in suboxic conditions at the seafloor (Kietzmann et al., 2014). The presence of ash beds, concretions, and high TOC indicates periods of low sediment accumulation rate (e.g., Minisini et al., 2018). Within this motif, the largest bulk-volume hydrocarbon (both in the oil and gas windows) is associated with LF 1, 2, and 5, which are the lithofacies characterized by high TOC, abundant coccolith-rich pellets, and dispersed altered volcaniclastic material. This motif is considered "distal" because it is not diluted with large biological components (generally delivered by energetic bottom currents), and it corresponds to Facies Association 1 in Kietzmann et al., 2020, this Memoir.

Motif B (LF 2, 3, 4, 9, 10, 12)

Motif B occurs in the foresets of low-angle clinoforms (Units 1 and 2, Figure 2). This motif is characterized by the alternation of organic-rich mudstones, marlstones, and argillaceous limestones, commonly arranged in coarsening-upward cycles (0.4–2.6 m), which increase in carbonate content toward their tops. Primary depositional materials include bioclastic detritus and other biological components (i.e., radiolarians, saccocomid crinoids, bivalves, and ammonites—some of the latter are transported from shallow water), mudstone intraclasts, algal organic matter, coccolith-rich pellets, sponge spicules, and rare silt-size terrigenous grains. Ash beds and their diagenetic products are present but in less quantity than in Motif A. Motif B is interpreted as deposited within the distal to middle portions of the foreset (outer to mid ramp), just below the storm-wave base, under suboxic to oxic conditions at the seafloor. Most of the bulk-volume hydrocarbon is associated with LF 2. This motif corresponds to Facies Association 2 in Kietzmann et al., 2020, this Memoir.

Motif C (LF 7, 8)

Motif C occurs in steep foresets (>1°) (Figure 4) and is dominated by fine-grained siliciclastic components: clay minerals and silt-size feldspars, quartz, and Fe–dolomite grains. Dolostone and soft-sediment deformations are common. Ash beds are rare. Motif C is interpreted as deposited in the foresets of the younger clinoforms in relative higher-energy environments characterized by sediment gravity flows, slope instability, and pulses of early diagenesis. This motif corresponds to Facies Association 3 in Kietzmann et al., 2020, this Memoir. Overall, the reservoir quality of this motif is poor and is the worst among the three.

Motive Distribution and Hydrocarbon Distribution

Integrating the motifs derived from core descriptions with the well logs and the seismic data, two contrasting associations emerge: (1) the association of motifs A and B and (2) the association of motifs A and C (Figures 2, 4). The first association contains a succession of Motif A, interpreted as the basal transgression of the Vaca Muerta, hence corresponding to a backstepping of the lowermost unit (Unit 1), overlain by Motif B, defining a seaward-stepping prograding clinoform (a regression) with a very low angle, which is typical of a carbonate ramp (upper Unit 1) (Kietzmann et al., 2014, 2016; Rodriguez Blanco et al., 2017). The ramp is activated by a landward highly productive carbonate factory during a regression without subaerial shelf exposure (see figure 18 in Reijenstein et al., 2020, this Memoir). The second association contains Motif A overlain by Motif C that defines a clear progradation with higher-angle foresets and clear shelf break (Unit 4).

Hydrocarbon distribution is different within these two representative types of depositional systems. Within the gently dipping carbonate ramp setting (older system, Unit 1), the distribution of TOC-rich lithofacies (having the largest bulk-volume hydrocarbon) displays low lateral variability (in fact, Unit 1 is not a proper clinoform with shelf edge). By contrast, TOC-rich lithofacies within the younger system (Unit 4)

occur mainly in bottomsets and lower foresets, whereas deposits within the upper foresets lack reservoir potential as they were affected by slope instability, gravity flows, and high sediment accumulation rate, which diluted the organic matter and hampered the accumulation and preservation of high-TOC mudstone.

LITHOLOGICAL CYCLICITY

The Vaca Muerta motifs A and B display a decimeter-scale alternation between two main groups of lithofacies: "mudstones" (LF 1, 2, 4, 5, and 7) and "limestones" (LF 3, 6, and 9) (Table 1). Mudstones and limestones present similar texture and same grains (although in different percentage: Limestones present more than 60% of carbonate, whereas mudstones contain less than 40%) indicating that both lithologies formed by similar sedimentological processes, both in foresets and bottomsets (topsets display different facies and belong to the Quintuco Formation and hence are not considered here). A thorough description of components and cements of the microfacies is available in Kietzmann et al., 2020, this Memoir.

Limestones in the bottomsets consist of LF 3 and 6 ("intraclastic grainstone" and "radiolaritic wackestone" in Kietzmann et al., 2020, this Memoir). Limestones in the foresets consist of LF 3 and 9 ("intraclastic grainstone" and "heterolithic marlstone to limestone" in Kietzmann et al., 2020, this Memoir). Mudstones in the bottomsets consist of LF 1 and 2 ("organic-rich mudstone" and "bioclastic wackestones/packstones" in Kietzmann et al., 2020, this Memoir). Mudstones in the foresets consist of LF 4 and 7 ("epistominid wackestone" and "organic-lean mudstone" in Kietzmann et al., 2020, this Memoir).

The main sedimentological processes related to limestones and mudstones are suspension and bedload transport by bottom currents and gravity flows, fallout, and early diagenesis. The diagenetic overprint is more common in the limestones than in the mudstones. The cyclic alternation between limestones and mudstones in the bottomsets and foresets occurs every 1 to 3 m (3–10 ft). In the topsets, cycles are poorly developed, probably because of the high bioturbation, high energetic currents, and diagenetic effects that obliterated them. In Unit 5, where cores exist for all depositional sectors (topset, foreset, and bottomset), the average thickness of the cycles increases basinward. As the bottomsets contain abundant bedding-parallel concretions, it is likely that sediment accumulation rates were null or sufficiently low, so that pore waters could be supplied by solutes from the overlying water column through diffusion (Macquaker et al., 2014). The presence of early strata-bound cements profoundly impacts the mechanical properties of the rock by introducing significant compositional and fabric heterogeneity. Even within the bottomsets, the average thickness of the cycles increases basinward, that is, in Unit 2, six cores retrieved from the bottomset show cycles thickening from 1 to 2.6 m (3–8.5 ft). These cycles are interpreted as representing changes in the Earth's circumnavigation of the Sun or Milankovitch Cycles. Each cycle has a specific duration, and when the measured cyclic sections are tied to the ages provided by magnetostratigraphy or biostratigraphy, they provide a precise chronometer where each cycle represents 20, 40, or 100 Ky (Leanza et al., 2020, this Memoir) and hence represent fifth-order cycles (*sensu* Vail et al., 1977).

All the observations on the cyclicity may have implications in defining the geomechanical units. In fact, the cyclostratigraphy quantifies and characterizes the alternation of lithologies with strong mechanical contrast (vertical heterogeneity). Recognizing the stacking pattern and distribution of this vertical heterogeneity allows predicting the hydraulic fracturing behavior (e.g., pinch points, pancake fracks, tortuosity, etc.) and the associated stimulated rock volume (SRV).

At seismic scale, the contrast of acoustic impedance between alternating stratigraphic units also influences the stimulated rock volume (this unit could represent fifth-order cycles, recurring every 200–500 Ky). The acoustic impedance of the different stratigraphic intervals along the clinoform are calibrated with lab measurements of acoustic velocity, porosity, and density performed on core plugs (see figure 4 in Reijenstein et al., 2020, this Memoir). Once calibrated, the acoustic impedance provides a guide for evaluating the quality and heterogeneity of the organic-rich intervals, thus indicating the most appropriate landing zones.

SEDIMENTARY AND BIOGENIC STRUCTURES AND PROCESSES

The cores in the blocks Cruz de Lorena (CdL x-3) and Sierras Blancas (SB x-1001) recovered rock from the foresets (outer to middle ramp), whereas the cores in El Trapial block (ET-1, ET-2, and ET-6) recovered rock from the bottomsets (distal ramp) (Figure 2). All cores represent coeval strata (Unit 1 and Unit 2). Millimeter-scale descriptions of the cores reveal that sedimentological patterns in the foresets are different than those in the bottomsets.

Foresets Characterization

The foresets of Motive B show recurrent lithologies presenting self-similar sedimentary structures, trace fossils, and bioturbation index (belonging to LF

3 and 9 when core described at decimeter scale, see Table 1). LF 3 and 9 are encased in LF 2.

Lithofacies

LF 3 and 9 consist of calcareous mudstone, marlstone, and argillaceous limestone that can be subdivided into sublithofacies: LF 3 includes sublithofacies MCl (parallel-laminated coarse mudstone with tabular or lenticular and massive or normal-graded beds) and minor MCrb (erosive to sharp-based, ripple cross-laminated coarse mudstone with thin beds and laminae commonly delineated by organic-rich rip up clasts). MCl are encased in fine mudstone.

LF 9 includes sublithofacies MCl and MCrb, with minor MCrl (lenticular to tabular, discontinuous, and coarse mudstone laminae showing downlapping relationships with the underlying surfaces), Mi (erosive-based, thin-bedded, and massive marlstone and tabular organic intraclastic conglomerate, overlain by very thin-bedded, parallel-laminated, coarse-grained, and medium-grained marlstone couplets) and Mc (erosive, sharp to gradational-based, thin-bedded, and massive to normally graded marlstone to limestone with intervals of sand-size calcareous material showing intrabed erosive surfaces; both basal and intrabed erosive surfaces are represented by (1) a very thin-bedded, tabular, lenticular or gutter-shaped, and coarse-grained marlstone interval or (2) a ripple cross-laminated, coarse-grained marlstone).

Locally, mudstone pseudo-nodules and pyrite occur within the marlstone. Locally, carbonaceous material delineates parallel lamination or is concentrated in very thin lags. All sublithofacies are generally encased within the background sublithofacies Mm (very thin to thin-bedded, massive, medium-grained to fine-grained marlstone).

Sublithofacies MCl, MCrl, and MCrb were produced by mud-rich unidirectional currents generating tractive sedimentary structures with poor sediment supply. Specifically, the coarse mud lags of MCl represent migrating ripples in sand-starved conditions (similar to "ripple tails" of Schieber et al., 2013). Sublithofacies Mi record deposition from turbidity currents, showing bedload transport of silt-size clasts and organic matter debris. Sublithofacies Mc was deposited by mud-rich sediment-gravity flows with evidence of fluid mud and waxing to waning energy patterns. The background sublithofacies Mm represents hemipelagite.

Ichnology

Trace fossils are subdivided into three trace fossil assemblages: the *Bergaueria–Lockeia*, *Nereites missouriensis*, and *Palaeophycus heberti.* The *Bergaueria–Lockeia* assemblage comprises *Bergaueria* isp., *Lockeia siliquaria, Skolithos* isp., *Teichichnus rectus*, and escape structures. Commonly, *Bergaueria* and *Lockeia* can be vertically associated with a second colonization event, indicating an *Equilibrichnia* ethology after erosive events. The *Nereites missouriensis* assemblage consists of *Nereites missouriensis, Phycosiphon incertum, Planolites* isp., *Palaeophycus* isp., *Palaeophycus heberti*, and *Asterosoma* isp. generating moderately to highly bioturbated intervals. The *Palaeophycus heberti* assemblage is restricted to highly bioturbated, completely homogenized intervals and is represented by *Palaeophycus heberti* and *Planolites* isp.

Bioturbation patterns

Nine cycles of sublithofacies are identified within the studied foresets (outer to middle ramp) and are subdivided into environments of deposition with low energy (corresponding to LF 3), moderate energy (no correspondence), and high energy (corresponding to LF 9) (Figure 6). Low-energy cycles comprise intervals 0.5 m (1.6 ft) thick constituted by the sublithofacies MCl. Moderate-energy cycles are 1 to 10 m (3 to 33 ft) thick and consist of the sublithofacies MCl, MCrb, MCrl, Mi, and Mm (Figure 6B). Both the low- and moderate-energy cycles display a decrease in bioturbation index at the base, from 4–6 to 0–2, and an increase toward the top. High-energy cycles (5–10 m [16–33 ft] thick) display variable bioturbation indexes, have a predominance of the sublithofacies Mc, are characterized by the *Bergaueria–Lockeia* assemblage, and occur stratigraphically higher in the section (where prograding foresets present steeper slopes, see Figure 6B).

Paleoecology and origin of the foreset cycles

Sedimentological and ichnological observations allow recurrent paleoecological limiting controls in bioturbation to be differentiated within the cycles defined. Hydrodynamic energy, sediment accumulation rate, and oxygenation are the controlling factors for trace fossil development. The higher the bioturbation index, the lower the energy and sedimentation rate in the environment (as far as oxygen is present in the sediment). This inverse correlation is driven by a long time span of colonization at the beginning of cycles and a short time span of colonization at the end of cycles when the energy in the environment of deposition increases. The middle part of the cycles represents the highest-energy condition and shows preservation of sedimentary structures (including current ripples) because of the low degree of bioturbation. In addition, the *Bergaueria–Lockeia* assemblage displaying *Equilibrichnia* structures indicates that these burrows

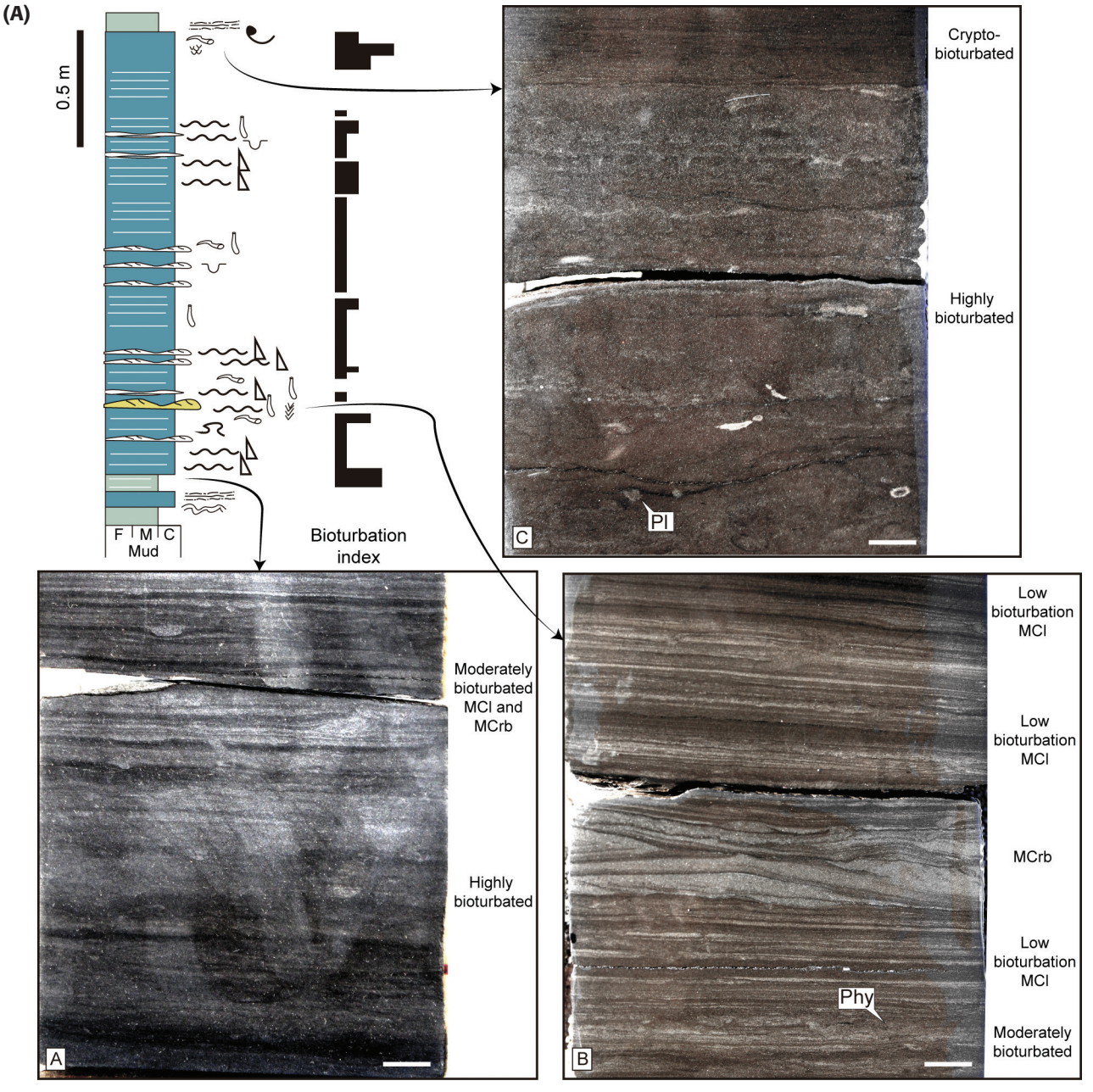

Figure 6. On this page: Moderate-energy cycle displaying the typical upward pattern of (A) mottled mudstone with bioturbation decreasing upward, (B) moderate to low bioturbation lithofacies, and (C) highly bioturbated mudstone capped by cryptobioturbated intervals. Next page: Stratigraphic sections showing lithology, bioturbation index, and, low-, moderate-, high-energy cycles. Well 1 is CdL x-3, well 2 is SB x-1001. See stratigraphic location of cores in Figure 2. MCl: parallel-coarse mudstone laminae; MCrb: ripple cross-laminated coarse mudstone; Phy: *Phycosiphon* incertum; Pl: *Planolites* isp.

migrated vertically to adjust to newly deposited sediment. This behavior suggests the existence of organisms capable of keeping pace with sedimentation rates and maintaining open connections to the seafloor, possibly indicating suspension feeding strategies (Mángano et al., 1998). The return to oxygen-deficient conditions at the end of the cycles indicates that the energetic conditions are coupled with ventilation of the seafloor that supported the described ichnofauna.

It is proposed that the sedimentary processes related to these variable bioturbation indexes in the foresets (outer to middle ramp) are associated to bottom currents. The evidences that support this interpretation are the existence of highly bioturbated intervals,

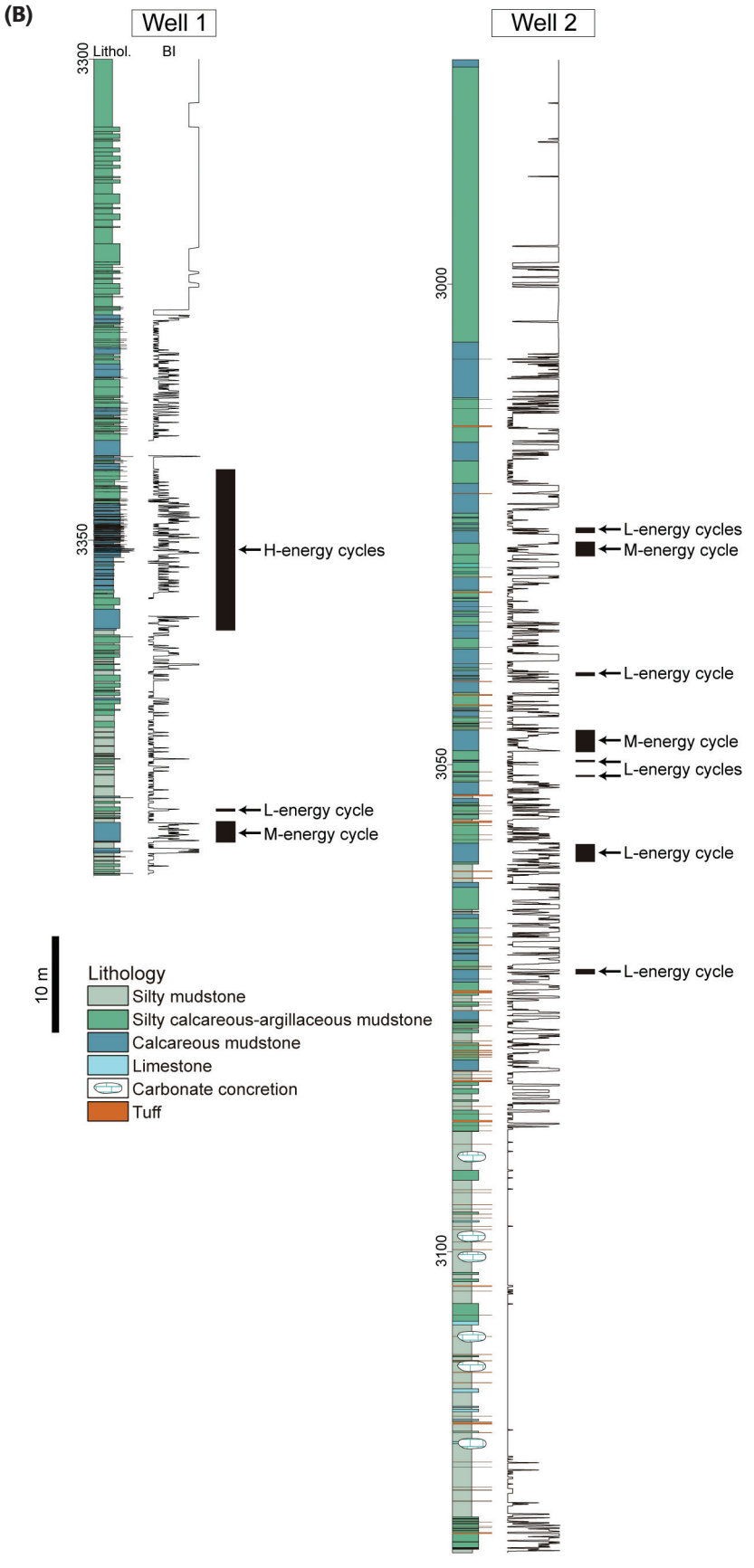

Figure 6. (Continued)

the bi-gradational sequence (increasing to decreasing energy pattern) (Rebesco et al., 2014), the abundance of tractive sedimentary structures (MCl, MCrb, and MCrl), and the seismic geomorphology showing contourites along the foresets (Reijenstein et al., 2020, this Memoir).

Bottomsets Characterization

Within the bottomsets, the depositional sector with the highest resource density, organic-rich mudstones (LF 1 and 2), and argillaceous limestones (LF 6) represents approximately 80% of the stratigraphic column (Figure 4). The bottomset facies are more difficult to interpret, with respect to the foreset facies, because they show little lithological contrast, mainly represented by dark-coloured mudstones with subtle sedimentary structures (e.g., faint current mud ripples).

In fact, during burial, the water-rich mud compacts (e.g., Enos and Sawatsky, 1981; Goldhammer, 1997; Lash and Blood, 2004) and the sediment dewaters losing up to 90% of its volume in the first few meters of burial (e.g., Schieber, 2011). The depositional fabrics are profoundly altered by dewatering, making it difficult to decipher the sedimentary products and to determine the original processes responsible for sediment emplacement. Furthermore, during burial, the physical compaction flattens beds and laminae geometries and may cause researchers to argue that deposition occurred in low-energy settings as a result of suspension settling from buoyant plumes (e.g., Potter et al., 1980) when instead the sediment was transported in bedload and accumulated as current mud ripples (e.g., Schieber et al., 2007, 2010; Schieber, 2011). This is particularly problematic if the rock develops a fissile fabric once exposed to weathering in the outcrop as the fissility (typical of shales) may be confused with lamination, too (e.g., Schieber et al., 2007). Therefore, we avoid naming the Vaca Muerta a shale; we call it instead a mudstone.

All of the aforementioned problems may be avoided where the TOC-rich bottomsets of the Quintuco–Vaca Muerta system develop a peculiar facies that

preserves an almost uncompacted record of primary sedimentary structures, that is, the bedding-parallel, early-diagenetic carbonate concretions (Gómez Rivarola and Borgnia, 2018; Kietzmann et al., 2016; Otharán et al., 2018) formed near the sediment–water interface in response to microbial decay of organic carbon (LF 12 in Figure 5).

The precipitation of early cements in response to microbially mediated oxidation of organic matter in the oxic and the sulfate reduction zones commonly reduces compactional porosity. This reduction occurs because the cements precipitate in pore waters that are in diffusional contact with the overlying water column. Diffusion supplies the necessary oxidants (particularly oxygen and sulfate) to the reaction sites associated with the microbial-mediated oxidation of organic carbon in the surficial water-rich pore fluids (e.g., Macquaker and Gawthorpe, 1993; Westphal et al., 2000; Dong et al., 2008). Enough solutes to form a large concretion to fill the available water-filled pore space can only be transported to reaction sites during prolonged breaks in sediment accumulation. Once the concretions form, they resist compaction and differential compaction occurs as the grains surrounding the concretions rotate from a card-house fabric toward a fissile fabric (e.g., Lash and Blood, 2004; Marshall and Pirrie, 2013). With the chemical requirement to supply large volumes of organic carbon and null or low sedimentation rates (e.g., Aplin and Macquaker, 2011), it is not surprising that the bottomsets of the Quintuco–Vaca Muerta system record 5 to 20 cm thick concretions occurring every 2 to 5 m [7–16 ft] in the stratigraphy (Figure 7).

Carbonate Concretions

The following description of concretions is made on hand specimens from the outcrops (Arroyo Mulichinco, Río Neuquén, Tres Chorros, Picún Leufú) and cores (El Trapial block) belonging to Unit 1 and the lower part of Unit 2. The cores of El Trapial block document that the vertical frequency of the concretions increases basinward: from one concretion every 4.0 m (13 ft) of stratigraphy to one every 2.5 m (8 ft) and to one every 1.8 m (5.9 ft). The understanding of this trend is useful when considering the input for the geomechanical units. In fact, not only the frequency but also the width, height, and space between concretions may be determined. For example, concretions with similar genesis in the Eagle Ford

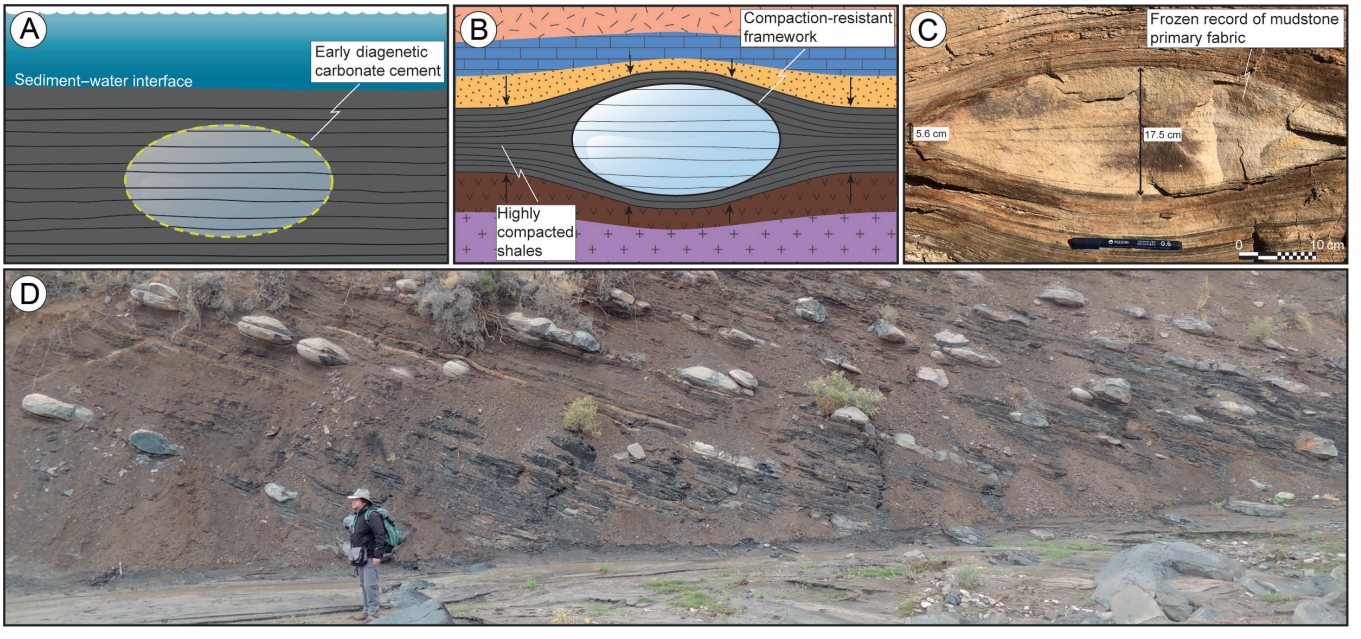

Figure 7. Early diagenetic calcareous concretions provide an archive for analyzing mudstone transport and depositional processes. (A–B) Line drawing explaining the origin of a carbonate concretion: (1) deposition of organic-rich, fossiliferous mud, (2) precipitation of carbonate cement in pore spaces determining concretion growth, and (3) burial and differential mechanical compaction. (C) Early diagenetic concretion from the Vaca Muerta Formation. Note the differential compaction between the concretion (thickness of original deposit 17.5 cm [6.9 in.]) and the mudstone layers deforming around it (5.6 cm [2.2 in.]). (D) Well-defined stratal horizons of early diagenetic calcareous concretions surrounded by highly compacted organic-rich mudstone (average TOC 4%, maximum TOC 8%) in the basal Vaca Muerta Formation (modified from Otharán et al., 2020).

unconventional play (Texas), appearing as discoidal bodies parallel to bedding, register a width between 0.5 and 2.5 m (1.6–8 ft), thickness from 7 to 15 cm (3–6 in.), and average horizontal distance among them at 1 to 2 m (3–7 ft) (Minisini et al., 2014). These values and shapes are similar to the concretions described in the outcrops of Vaca Muerta, where the average distance between concretions is from 3 to 5 m (10–16 ft), average width is between 2 and 4 m (7–13 ft), and average thickness is 30 cm (12 in.). From the description of cores and outcrops, it is observed that the thickness and the shape of the concretions in Vaca Muerta remain similar, whereas the width may vary considerably.

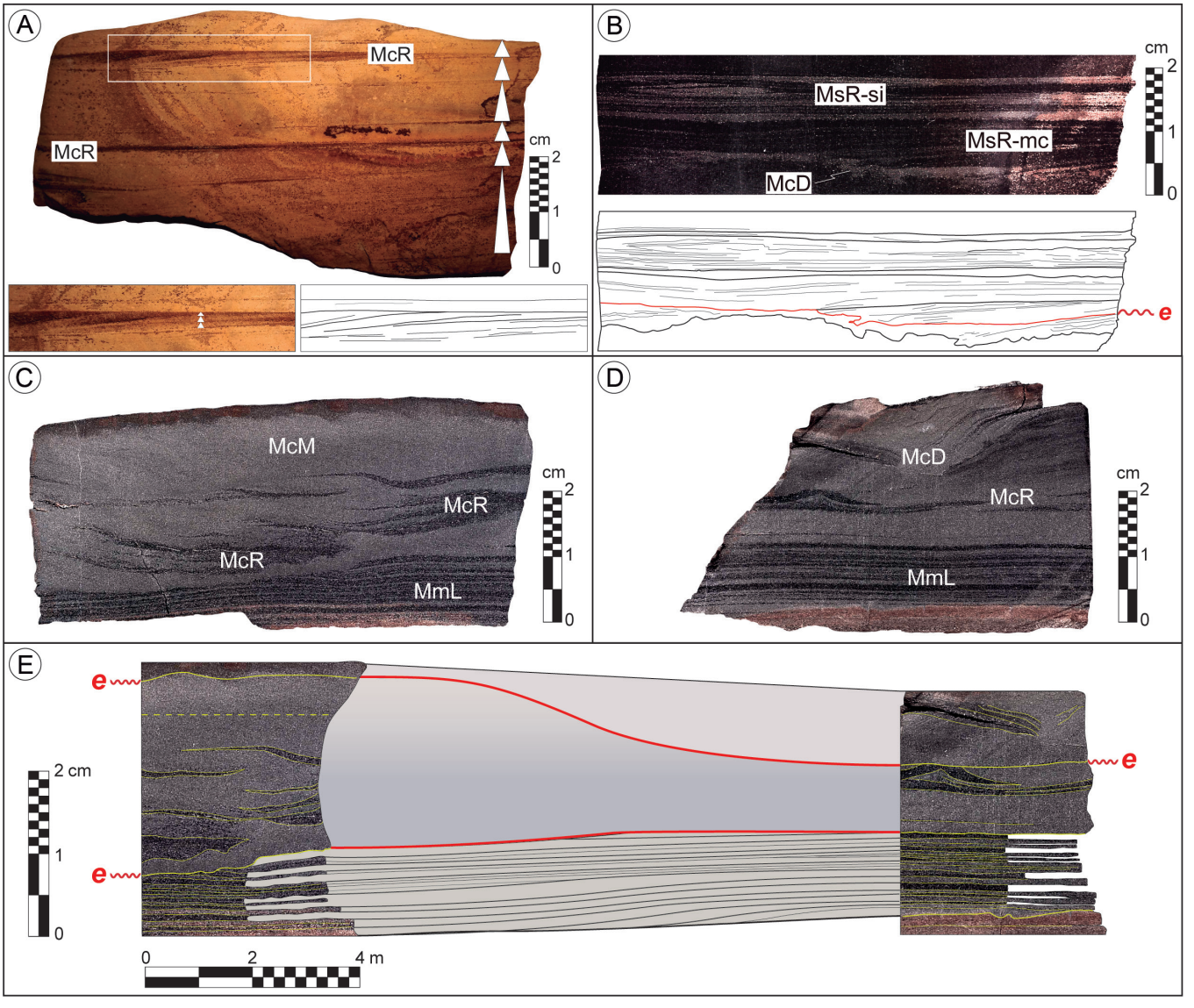

Figure 8. Primary sedimentary features preserved inside early diagenetic carbonate concretions. (A) Normally graded mudstones exhibiting current-generated ripples (McR). (B) Soft-sediment deformation structures (McD) topped by an erosional surface ("e") and a mudstone bed with internal lamina truncations. (C–D) Two samples from different concretions within the same horizon (10 m [33 ft] apart) showing bottom-up, medium-laminated mudstones (MmL) sharply overlaid by rippled coarse-grained mudstones (McR) composed of mud rip-up clasts. Note in (C) that the rippled mudstones are gradationally overlain by massive coarse-grained mudstones (McM), whereas in D they are truncated by coarse-grained mudstones displaying soft-sediment deformation (McD). (E) Correlation between (C) and (D) showing the complexity of mudstone-event beds (Otharán et al., 2020). e = erosional boundary; McD = coarse-grained mudstones with soft-sediment deformation; MmL = parallel-laminated medium mudstones; McM = massive coarse-grained mudstones; McR = rippled coarse-grained mudstones; MsR-mc = muddy-clast-rich and rippled-sandy mudstone; McR-si = interlamination of silt grains and mud aggregates.

The main primary sedimentary structures recognized in the analyzed concretions include (1) current-generated mud ripples (MsR, Figure 8A, B); (2) planar, continuous-to-discontinuous parallel lamination with occasional low-angle lamina truncations (MfL, MmL, Figure 8C, D); and (3) massive (MfM, Figure 8C; McM, Figure 8E). Current-generated mud ripples are similar in shape, size, and components to those described from experiments in laboratory flumes (e.g., Schieber et al., 2007). Ripples can be composed of an interlamination of coarse silt grains and mud aggregates (Figure 8A, B), or alternatively they can be entirely composed of sand-size soft mud aggregates (e.g., fecal pellets, mud rip-up clasts) that are hydrodynamically equivalent to coarse silt grains (Figure 8C, D). Microfossils (e.g., forams, calcispheres) can be additional components of current-generated mud ripples.

Ripples on the lee side commonly downlap onto a sharp, scoured surface (McR in Figure 8C) creating ripples that overlay parallel-laminated mudstones (MmL in Figure 8D). Upwards, this rippled coarse-grained mudstone (McR) interval is transitionally overlaid by dark-colored, fine-grained "structureless" argillaceous mudstones, defining an apparent fining-upward deposit (Figure 8A). These fine-grained mudstones represent organic-rich deposits (up to 6% TOC) between 0.5 and 4 cm (0.2–1.6 in.) thick, and they may reach the top of each event bed. However, some mudstone-bed events display a complex stacking pattern characterized by an apparent fining-coarsening upwards laminae as well as vertical facies recurrence between massive, parallel-laminated and rippled mudstones, building up composite mudstone beds. Contrary to the event beds in the foresets, the bioturbation index within the concretions formed in the bottomsets is generally low. The aforementioned primary sedimentary structures suggest an accumulation from low-density turbulent muddy flows transporting fine-grained material mainly in bedload, probably ignited upslope by the combined effect of gravity, currents, and waves, as documented in modern systems by Macquaker et al. (2010) and Denommee et al. (2016). Some potential processes responsible for delivering mud to the bottomsets are (Figure 9) (1) muddy hyperpycnal flows (Mulder and Alexander, 2001; Zavala and Arcuri, 2016); (2) surge-type muddy turbidity currents similar to the "unifites" of Blanpied and Stanley (1981) and the "turbiditic mud layers" of Rupke and Stanley (1974); (3) storm-induced currents (Aigner and Reineck, 1982); (4) wave–current-aided sediment gravity flows (Bhattacharya and MacEachern, 2009) and wave-enhanced sediment gravity flows (Macquaker et al., 2010); and (5) cascading density currents (Wilson and Roberts, 1992, 1995). The internal layering and stacking pattern of some concretions analyzed suggest an origin related to muddy hyperpycnal flows, especially in the southern margin of the basin (Picún Leufú area).

The diagnostic criterion for a hyperpycnal origin of the concretion-hosted deposits is the presence of fining- and coarsening-upward trends at lamina scale, internal lamina truncations, and vertical alternation of parallel-laminated, rippled, and massive mudstones (Figure 10A). Such sedimentary features are commonly interpreted as related to flow velocity fluctuations during sustained periods of hyperpycnal fluvial discharges (Figure 10B) (Mulder and Alexander, 2001; Mulder et al., 2003; Nakajima, 2006; Soyinka and Slatt, 2008; Bhattacharya and MacEachern, 2009; Wilson and Schieber, 2014, 2015; Lash, 2016). Sustained fluvial discharges may be associated with long rivers flowing

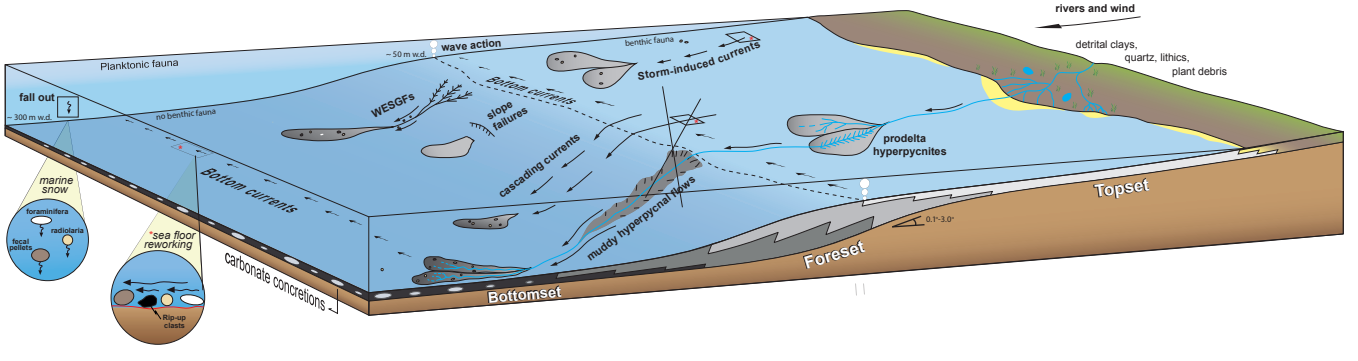

Figure 9. Block diagram illustrating some of the potential processes delivering mud to the bottomsets of the Vaca Muerta-Quintuco system. WESGFs: wave-enhanced sediment gravity flows.

in the flat lands of Gondwana, east of the Neuquén Basin (Ramos et al., 2020, this Memoir), and their erosion of the topset is one of the processes (together with tides, winds, and storms) responsible for the biogenic components found as reworked biogenic debris in the bottomset. Depending on the duration of the high-density fluvial discharge, the resultant muddy hyperpycnal flows may be sustained for days, weeks, or months (Mulder et al., 2003; Nakajima, 2006; Zavala et al., 2006; Soyinka and Slatt, 2008) resulting in long-lasting muddy underflows.

The upward coarsening and upward fining trend at lamina scale is a key diagnostic criterion to assign hyperpycnal origin to the concretion-hosted deposits. As recognizing upward coarsening and upward fining might be interpretative, an alternative view would be to describe those trends as laminae couplets where each laminae is characterized by specific grains: quartz and feldspar grains in the coarse silt-size laminae and aggregate grains composed of clay minerals and coccoliths in the fine-grained laminae. In this view, the lamination style may simply reflect changing ripple provenance with one ripple train being composed of quartz and the next by aggregate grains, without the implication of waning or surging flows related to the hyperpycnal flows (Yawar and Schieber, 2017).

Beyond muddy hyperpycnal flows, where an event bed internal stacking pattern is characterized by an overall normal grading trend (a basal massive/rippled coarse-grained mudstone interval (McM) overlain by massive, fine-grained mudstone deposit (MfM)), its origin may be associated to waning, surge-type intrabasinal muddy turbidity currents (Otharán et al., 2018). Intrabasinal muddy turbidity currents are products of episodic (non-steady) events triggered by slope instability or intense wave activity during storm events, effective processes delivering mud from the topset and foreset to the bottomset. These waning flows progressively lose their capacity and competence and deposit their sediment load as normally graded mudstone beds in distal foresets and proximal bottomsets locally associated with mass transport complexes (Arregui, 2014; Pose et al., 2014; Reijenstein et al., 2017; Otharán et al., 2018). As these flows require the existence of a depositional gradient, it is likely that they originated along the steep western margin of the basin, close to the active volcanic arc, rather than along the eastern margin where low-angle ramps (0.2°–0.3°) characterized the basin, especially during deposition of Unit 1 and 2.

The low bioturbation index within the studied mudstones could be associated not only to the typical dysoxic environment of the bottomsets, but also to the physical stress caused by the pulses of muddy underflows that rapidly deposited and buried the fine-grained materials (including the organic matter which, with this process, avoided the potential degradation by the benthic meiofauna).

Erosional features in mudstones: Insights for understanding mud delivery mechanisms

The recognition of erosional features in ancient mudstone successions has been historically underestimated because of the long-held fallout paradigm (e.g., Pettijohn, 1975; Potter et al., 1980). Nevertheless, increasing sedimentological evidence from ancient mudstone strata suggests that punctuated erosional events were common in the geological past (Schieber, 1998, 2003; Macquaker et al., 2007; Schieber et al., 2010). Beyond the primary sedimentary structures described herein, concretion-hosted mudstone layers show a variety of post-depositional sedimentary structures that give hints on primary mud deposition, erosion, and redeposition in the bottomsets. Most of the studied samples show a basal erosional boundary, and depending on the magnitude of the erosion, they can exhibit (1) soft-sediment deformation structures developed in shallow souplike muddy substrates (flame and convolute lamination, Figure 8B) and (2) flute marks (Figure 10A) related to the erosion of deep, cohesive, and strength-firm muddy substrates (Allen, 1969). Flute marks suggest a flow separation under severe velocity conditions capable of eroding the cohesive and firm muddy substrate (Allen, 1969), hence incorporating the intrabasinal eroded material to its sediment load and transporting it basinward. On the contrary, soft-sediment deformation structures underneath an erosional surface suggest an overpassing flow weaker than in the previous case, thus enabling a partial preservation of the uppermost soupy mud level (Sanders, 1965). Flume experiments developed by Einsele et al. (1974) have demonstrated that water-rich muds (70 vol.%) required overpassing flow velocities of 150 cm/s to produce soft-sediment deformation structures because of the drag forces exerted on the sediment surface (Schieber, 1998).

Mud bottom erosion would be enhanced at topsets with the consequent incorporation of the eroded materials (e.g., muddy rip-up clasts, fossil debris, organic matter, etc.) into the sediment load of the flow (Figure 8). These fine-grained sediments would be transported over long distances (~200–250 km [~120–155 mi]) toward the distal bottomset, where they would be finally accumulated as compositionally mixed mudstone beds. These processes have been recently recognized in organic-rich muddy sediment cores recovered from the distal part of the modern

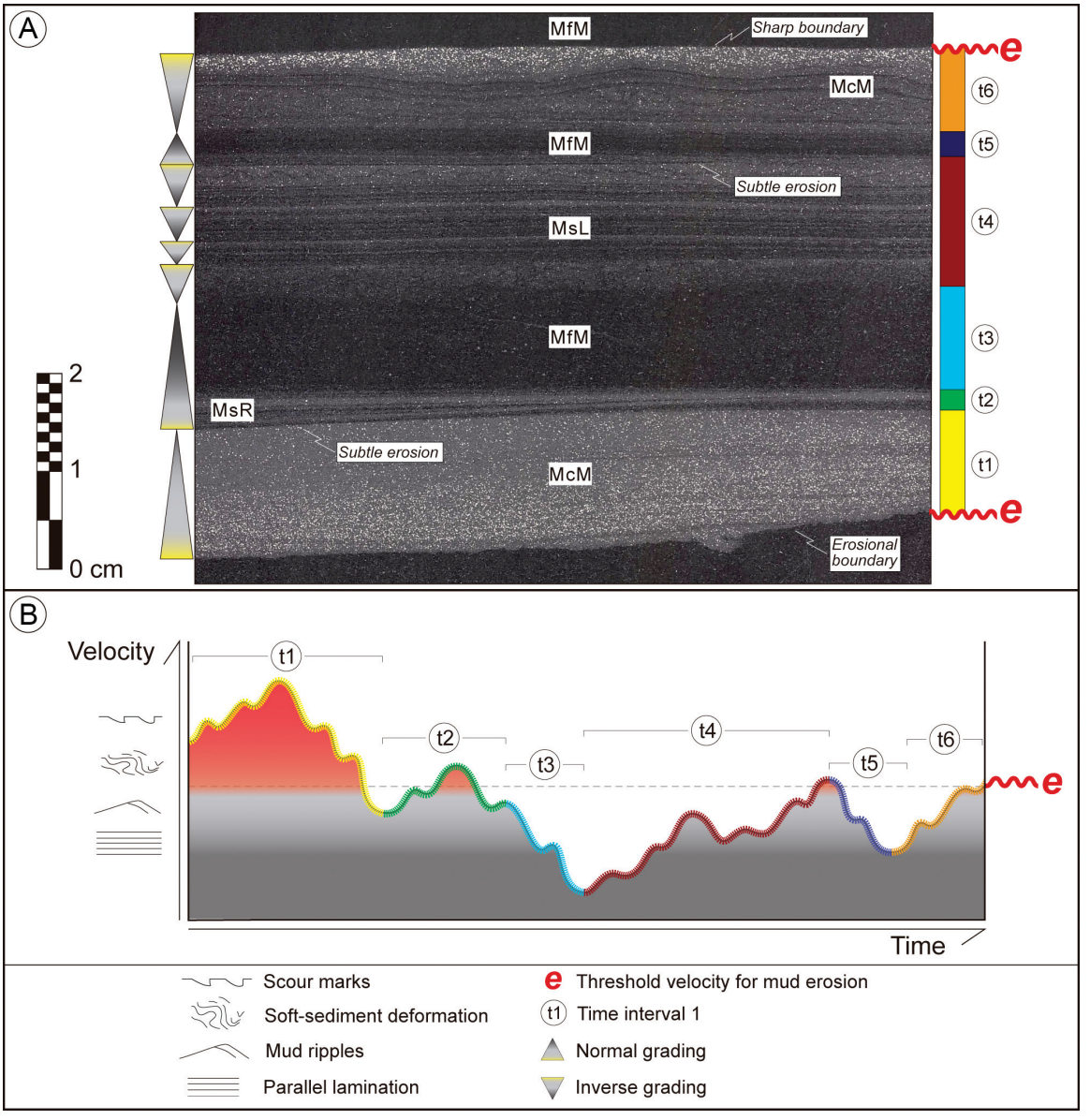

Figure 10. (A) Composite mudstone bed characterized by repeated fining-coarsening upward trends and subtle internal erosional features at lamina scale. (B) Flow velocity fluctuations occurred during the accumulation of the composite mudstone bed in (A), interpreted as deposited in a punctuated, long-lasting muddy hyperpycnal flow event (Otharán et al., 2020). McM = massive coarse-grained mudstones; MfM = massive fine-grained mudstones; MsL = parallel-laminated sandy mudstones; MsR = rippled-sandy mudstones.

Ogooue turbidite system (Biscara et al., 2011; Mignard et al., 2017) as well as in the modern Congo mud-rich deep-sea turbidite system (Baudin et al., 2010, 2017a, b; Stetten et al., 2015). Beyond the mixed mudstone beds, the carbonate mud in the fine-grained carbonate beds of the Vaca Muerta bottomsets also occasionally form a thick succession of limestones (e.g., Los Catutos Member) derive from the carbonate-rich topsets (Rodriguez Blanco, 2016; Rodriguez Blanco et al., 2017). On modern shelves and carbonate platforms, not only the daily energy regime of tides and winds but also storms stir up sediment causing the density of the platform water to increase and subsequently to form cascading density currents (Wilson and Roberts, 1992, 1995). Cascading density currents flow for days and thus are similar to hyperpycnal flows. The flow path of cascading density currents is influenced by (1) the contrast between their density and the density of the surrounding water masses and (2) the current flows along pycnoclines (Eberli and Betzler, 2019).

The sediment transported by the cascading currents can flow tens of kilometers before being admixed to the ambient current system (Pilskaln et al., 1989). Once admixed, these off-bank sediments can be further transported by contour currents and bottom currents (Betzler et al., 2014).

Correlation Bottomsets-Foresets

Facies

Organic-rich mudstones (LF 1 and 2) and argillaceous limestones (LF 6) are the typical facies of the coeval units retrieved in the three cores from El Trapial block, belonging to the distal bottomset, and in the Aguila Mora core, belonging to the proximal bottomset (Motif A in Figure 4). The three cores in El Trapial block are approximately 15 km (9 mi) apart and provide a clear example of the lateral correlation at bed scale where not only the sedimentological characteristics but also the thickness of the beds remains the same, suggesting that the sediment accumulation rate and the sedimentary processes were self-similar in that area of the distal bottomset. Instead, the coeval distal foreset (in Sierras Blancas core SB x-1001) presents limestone-dominated facies, whereas the coeval proximal foreset (in Los Catutos outcrop, 150 km (90 mi) southwest of Sierras Blancas core) presents 70 m (230 ft) of thick-bedded bioturbated limestones encasing a 10 m (33 ft) thick marlstone with gravity-flow deposits. This 70 m thick unit in Los Catutos correlates with a 11 m thick mudstone unit in El Trapial cores. These observations provide a clear example of the significant variability in lateral facies at clinoform scale, highlighting the existence of multiple sedimentary processes at play.

Paleo water depth

The sedimentological features of cores and outcrops analyzed in the Vaca Muerta lack the signatures to characterize a precise paleo water depth. However, seismic data help estimate the paleo water depth of the bottomsets by measuring the relief between the top and the base of the foresets (estimated a minimum of 200–250 m [~650–820 ft] by Mitchum and Uliana, 1985). Data collected in the last decade allow an analytical backstripping of the clinoforms to attempt a better quantification of the paleo water depth of the bottomsets in relation to the topsets (Figure 11).

Part of the main seismic transect presented in González et al. (2018), already transformed from time to depth (bulk velocity of 4000 m/s), was here georeferenced and assigned an elevation profile. The six interpreted stratigraphic units (*sensu* Desjardins et al., 2018) were imported into Badley Geoscience's FlexDecomp tool for 2D flexural decompaction and backstripping. The Intravalanginian unconformity (top Unit 6) defined the reference level for the model (0 m water depth) as it is related to a sea level drop that placed the fluvial sandstones of the Mulichinco Formation atop the marine Vaca Muerta–Quintuco system. In all other units, the topsets of the Vaca Muerta–Quintuco system were assumed as indicators of the sea level (0 m water depth). Since the lithofacies of the clinoforms underwent different compaction during burial, each unit was split in a proximal limestone-rich sector (80% limestone, 10% mudstone, and 10% sandstone) and a distal mudstone-rich sector (10% limestone, 80% mudstone, and 10% sandstone) with assigned porosities, densities, and decompaction rates (derived from log data). The decay constant, the starting porosities, and the starting densities were automatically computed by FlexDecomp based on Sclater and Christie (1980). Time of deposition derived from ammonite biozones (see figure 5 of Minisini et al., 2020, this Memoir). A uniform crustal stretching factor (β) of 1.3 was applied across the whole section as background thermal subsidence to account for the rifting in the Pre-Cuyano cycle at 208 My.

With these general assumptions, and with an estimated error of 50 m, the model offers a first-order flexural unloading of the basin infill defining the following water depths for the proximal bottomsets (typical targets of the unconventional wells) (Figure 11): 350 m (1150 ft; top Unit 1), 300 m (984 ft; top Unit 2), 380 m (1280 ft; top Unit 3), 400 m (1310 ft; top Unit 4), 80 m (260 ft; top Unit 5), and 0 m (top Unit 6). Interestingly, the backstripped geometries placed the shelf break of top Unit 3 at approximately 50 m (~160 ft) water depth, coinciding with the same water depth inferred from the studies on the carbonate buildups, typical of the topset of Unit 3, both in seismic data and in outcrops (see Reijenstein et al., 2020, this Memoir).

Backstripping sequentially removes each sedimentary unit (note that in figure 11 the upper left plot is the youngest stage, and the lower right the oldest stage). At each stage, the topset is kept close to reference level (0 m), requiring base-level shifts. A land level rise (relative base level drop) going back in time implies a sea level rise going forward in time. Therefore, moving forward in time, from old to young reconstruction stages, the shifts imply: at least 270 m of sea level rise before the deposition of the base of Vaca Muerta, 150 m of sea level rise during deposition of Unit 1 (from T1 to T3), stillstand sea level during deposition of Unit 2 (from T3 to T5), 50 m of sea level rise during deposition of Unit 3 (from T5 to B2), 100 m of sea level rise

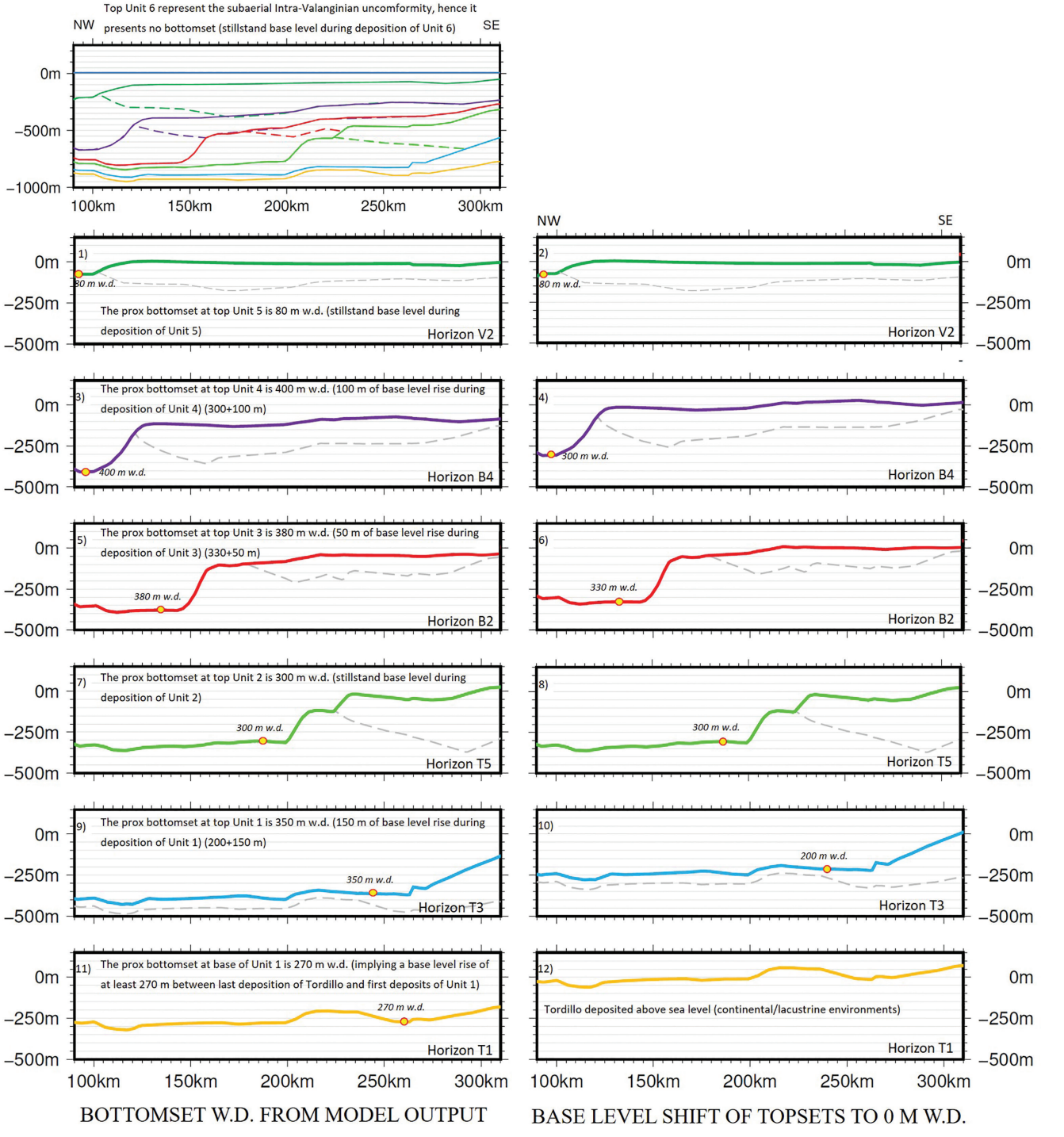

Figure 11. Backstripped profiles for the six units defining the Vaca Muerta–Quintuco system, depicting estimates of paleo–water depth at the time of deposition. A dashed line subdivides each unit into a proximal limestone-rich sector and a distal mudstone-rich sector with distinct porosities, densities and decompaction rates (Unit 1 presents only mud-rich lithology). Backstripping progressively removes layers from the top, back in time (from top left to bottom right, from 1 to 12). The resulting model output (stages 1, 3, 5, 7, 9, 11) needs to restore topsets to reference level (0 m) with a base-level shift (stages 2, 4, 6, 8, 10, 12). Labels are written to follow the basin infill history (from bottom left to top right, from 12 to 1). Profiles from seismic transect in González et al. (2018). w.d.= water depth

during deposition of Unit 4 (from B2 to B4), stillstand sea level during deposition of Unit 5 and 6 (from B4 to V4).

The model gives a first-order basin geometry through time in agreement with earlier studies on depth differences between topsets and bottomsets; it also provides new estimates of sea level fluctuations. Nevertheless, future work is needed to improve the control on uncertainties of the parameter space as well as issues related to the absolute base level (possibly related to negative dynamic topography, flexure, or waning thermal subsidence from the Jurassic rift phase).

DEPOSITIONAL MODEL

Literature and data analyzed so far have recorded that in the Vaca Muerta–Quintuco system biogenic carbonate originated in the shallow seafloor (topset) from benthic fauna (i.e., bivalves). The shallow-water benthic fauna was then transported offshore (foreset and bottomset). Biogenic carbonate also originated in the water column from planktonic fauna (i.e., nannoplankton, ammonites, and saccocomid crinoids), both in shallow and deep water (above topset, foreset, and bottomset). Biogenic quartz derived mainly from siliceous radiolaria living in the water column (above topset and foreset). Intrabasinal muddy rip-up clasts were created and transported by bottom currents and sediment gravity flows. Detrital quartz, as well as other siliciclastic material, reached the basin by wind and rivers, whereas volcaniclastic material entered the basin both as fallout from the volcanic activity and by wind and rivers that reworked the material deposited in subaerial environments (Kietzmann et al., 2014, 2016).

The carbonate, siliciclastic, and volcaniclastic material deposited at seafloor was then reworked by tides and bottom currents (e.g., cascading currents, hyperpycnal and turbiditic flows) moving sediment basinward from topset to foreset (Rodriguez Blanco, 2016; Rodriguez Blanco et al., 2017) and then captured by gyres and redistributed both along slope (perpendicular to the foreset progradation, Zeller et al., 2015b) and across slope (from foreset to bottomset, Kietzmann et al., 2016; Otharán et al., 2018). When the activity of currents was scarce, deposition by fallout was more common (Kietzmann et al., 2014; Otharán et al., 2018).

Diagenetic clays derived from the metastable volcaniclastic material, diagenetic quartz derived from the carbonate-replaced radiolaria, and diagenetic carbonate derived from the precipitation of the abundant carbonate material dissolved in the fluids flowing through the pore systems (see Kietzmann et al., 2020, this Memoir).

The very first deposits of the Vaca Muerta–Quintuco system overlay the Tordillo Formation that represented a near flat surface when the instantaneous transgression of the ocean flooded the Neuquén Basin. During the following sea level rise, the space of accommodation increased, and sediment was delivered from the margin toward the basin generating a low-angle ramp (0.2°–0.3°, Units 1 and 2) part of a carbonate system whose factory developed in shallow water with mainly biogenic material: skeletal grains (from planktonic fauna and shallow-water benthonic fauna, then transported from shallow to deeper waters, Kietzmann et al., 2014) and fecal pellets (produced by crustaceans mainly in the topset, Kietzmann and Palma, 2014). Then, clastic input, derived by wind and rivers, increased (Units 3 to 6). Once the sediment filled the accommodation space created at the topset by the sea level rise, the sediment could not deposit as a drape anymore and the hydrodynamic processes (waves, currents, gravity flows) became a key factor reworking the sediment basinward and reshaping the ramp into a prograding mixed carbonate–siliciclastic system with foresets between 1° and 3° (Mitchum and Uliana, 1985; Reijenstein et al., 2015; Zeller et al., 2015a; Kietzmann et al., 2016). When a distinguishable shelf break was created, salinity and density contrast in the water masses enhanced the current activity triggering hydrodynamic accumulations (banks, shoals) and in situ biohermal buildups in the distal topset. Banks and buildups formed an incipient lithified margin (typical of Unit 3) suggesting that nutrient levels and currents were suitable for widespread biological growth and extensive early cementation. Furthermore, the steep lithified margin was prone to sediment failures, producing mass transport deposits (see Reijenstein et al., 2020, this Memoir).

At a finer scale, within each unit, regressions (late HST to LST) recorded more carbonate, less siliciclastic and less organic material (e.g., Reijenstein et al., 2020, this Memoir), and in specific conditions (i.e., high sediment input in the southern sector of the basin), the trend was inverted and regressions recorded more siliciclastic and less carbonate material (Kietzmann et al., 2020, this Memoir). Other datasets in the southern sector report that siliciclastic input in the bottomset was (1) very high during sea level lowstands because of the erosion of the North Patagonian Massif, tipically represented by hyperpycnal sandstone lobes (Otharan et al., 2018; Paz et al., 2019); (2) high during transgressions because the accommodation space allowed the development of efficient currents on the topsets (typical along-strike currents) that reworked

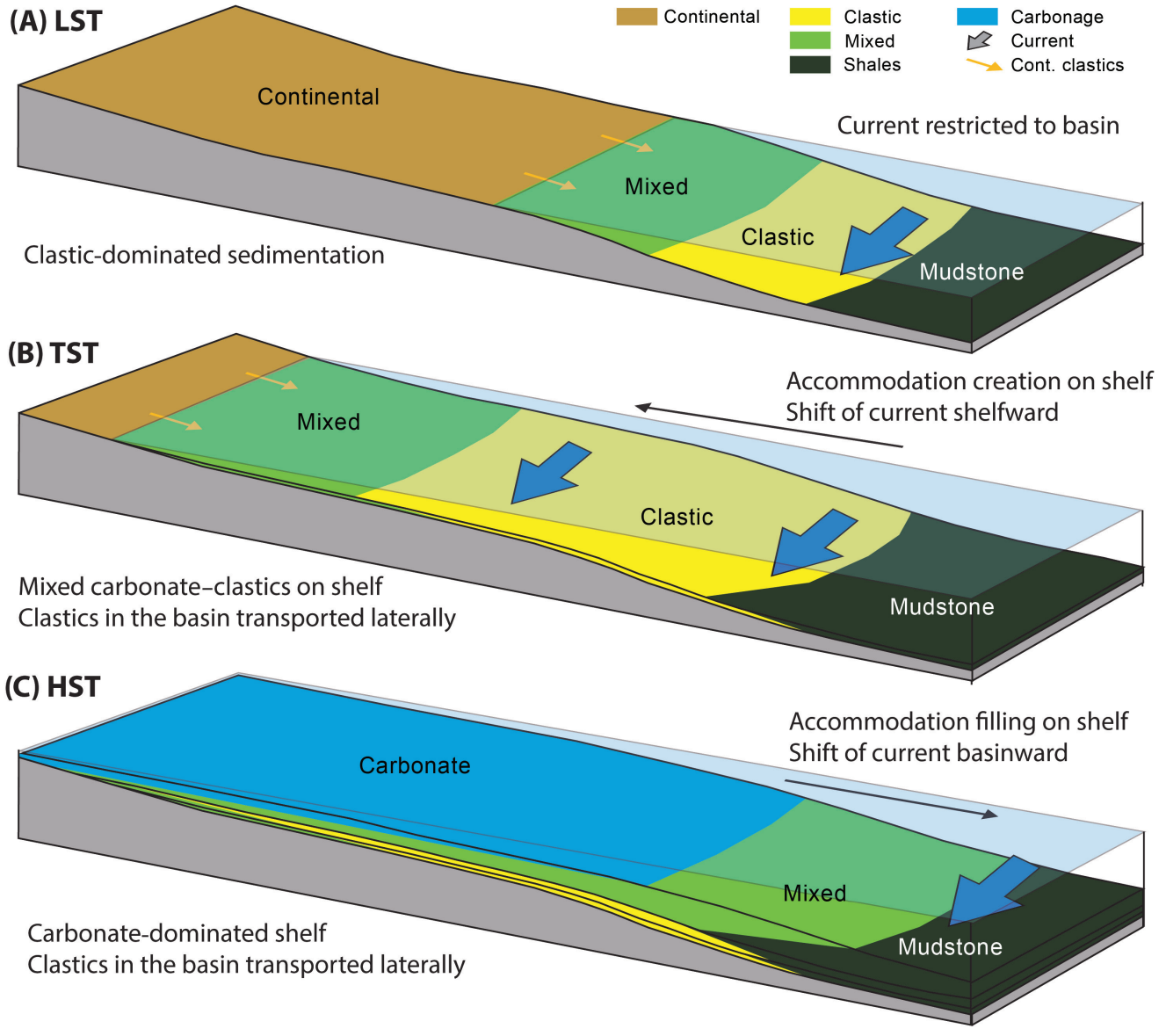

Figure 12. (A) During a sea level lowstand (LST), siliciclastic material is directly delivered to the basin, where along-strike bottom currents rework the fine-grained portion. (B) During transgressions (TST), accommodation space increases allowing along-strike current systems to develop on the shelf (topset) transporting and redepositing siliciclastic material. (C) During sea level highstands (HST), the lack of accommodation space hampers along-strike transport and the consequent siliciclastic delivery basinward (modified from Zeller et al., 2015b).

the siliciclastics both landward and basinward; and (3) low during sea level highstands because the accommodation was not enough to allow the development of currents capable of transporting siliciclastic material to the basin (Zeller et al., 2015b) (Figure 12). The variety of models explaining transgressions-regressions at sub-unit scale (fifth-order cycles) suggests the interaction of multiple contemporaneous local processes. It also highlights the need of further studies to reconcile the apparent controversies and better serve the facies prediction at this fine scale (same scale of the landing zone window and the vertical fracture growth).

Although the lateral facies variation is minimal in the distal bottomset (i.e., El Trapial block), local variations in thickness by the order of tens of meters over less than 5 km (3 mi) in the basin center are clear evidence of the influence of bottom currents (Weger et al., 2017). Considering the proximity to active subduction zones and reactivated inversion zones, the tectonic activity might have represented the main control on the sea level

fluctuation and, in turn, on the carbonate–siliciclastic mixing. Therefore, the triggers producing the clinoform progradation are: the increase in sediment input (controlled by climate) and the decrease in accommodation space (controlled by local tectonic movements and maybe global sea level fall).

The high-TOC stratigraphic units of the Vaca Muerta–Quintuco system deposited mainly in the bottomsets and lower foresets during recurrent periods of low sediment accumulation rate, basinwide suboxia–anoxia, and high bio-productivity, generally during transgressions (Figure 3) (see Domínguez et al., 2020a, this Memoir). Low sediment accumulation rates (2–8 cm/Ky [0.8–3.1 in./Ky]) were quantified through the absolute dating of volcanic zircons in ash beds (not presented in this chapter). The suboxia–anoxia was identified in previous works based on abundant framboidal pyrite, XRF analyses (e.g., V/(V+Ni) > 0.6), characteristic geochemical parameters (e.g., Th/U > 2) (Desjardins and Aguirre, 2018), lack of bioturbation (e.g., Kietzmann et al., 2011), and a negative shift of $^{13}C_{org}$ (Morettini et al., 2015). The higher bio-productivity in the early deposition of the Vaca Muerta Formation is inferred by the co-occurrence of (1) upward decrease of TOC, (2) upward decrease of (Ni + Cu)/Al, (3) increase of Al, and (4) constant P/Al ratios (see Brisson et al., 2020, this Memoir). The recurrent periods of low sediment accumulation rate, basinwide suboxia–anoxia and high bio-productivity created a stacking of high-TOC units generating a sedimentary wedge that thickened basinward (northwestward) with time, during the entire Vaca Muerta–Quintuco system, which lasted approximately 11 My (see representative Motif A in Figures 2, 3). The central sector of the basin presents the thickest wedge, whereas in sectors with less progradation and more aggradation of the clinoform (e.g., the northern and northeastern sectors), the thickness of high-TOC units is more uniform, resembling a drape more than a wedge. Basinwide, in the topset of the clinoforms, the erosional currents, the oxygenated water column and seafloor, and the high bioturbation negatively affected the preservation of organic matter, thus characterizing the upper part of the Vaca Muerta–Quintuco system with organic-lean units.

IMPLICATIONS FOR RESERVOIR QUALITY

TOC, Porosity, and Water Saturation

The TOC is a key reservoir quality indicator in the Vaca Muerta play. Lithofacies with the highest TOC (LF 1, 5, and 6) (Figure 13A) typically lack high concentrations of large biological components (bioclastic grains) and tend to dominate the bottomsets (Motif A). LF 2 and 3 show that low TOC is related to an increase in bioclastic grains, which is interpreted as an increase of the energy and the oxygen in the environment. LF 4, 7, and 8 are TOC lean and are interpreted as deposited in sectors with oxygenated sediment–water interface. Lithofacies with the highest TOC average values also have the highest porosity values; in fact, SEM images of LF 5 show that porosity mainly occurs within the organic matter (kerogen and abundant coccolith-rich fecal pellets). LF 2 shows porosity both within the organic matter and between carbonate grains (interparticle porosity). In LF 3, porosity is almost entirely interparticle (between bioclastic grains). LF 4 has the lowest porosity values and can be explained by its low TOC and its abundant, very fine-grained, and detrital carbonate in the matrix. LF 7 and 8 show high porosity associated to clays, and hence pores are numerous but small and disconnected.

In general, the lithofacies with the highest TOC and porosity have the lowest water saturations (Motif A, made of LF 1, 5, and 6). LF 2, 3, and 4 show higher water saturation, higher carbonate content, and lower TOC. The highest water saturation values appear in LF 7 and 8, but these values are related to clay-bound water as the facies are clay rich.

XRD

The XRD data provide information about the bulk mineralogy and when plotted in a ternary diagram display a pattern of values associated to the lithofacies (Figure 13B). However, bulk mineralogy alone is not enough to understand the main rock components (i.e., silica may be biogenic, clastic, or diagenetic). Therefore, XRD data are integrated with petrographic observations. LF 1, with the highest TOC, has a distinctive position within the ternary diagram: low carbonate content (< 30%), medium clay content (20%–40%), and high silica content (45%–65%). Thin sections show few bioclastic carbonate grains and a richness of detrital silt-size quartz and plagioclase grains. LF 2 displays more carbonate (up to 65%), which in thin section appears as bioclastic grains. LF 3 is rich in bioclastic detritus and other biological components (radiolarians, saccocomid crinoids, and bivalves) and has the highest carbonate content (40%–75%) and the lowest clay (< 30%) and silica content (10%–45%). LF 4 presents a dominant carbonate composition (75%–85%), abundant in the matrix, and low clay (< 25%) and silica content (30%–45%). LF 5 and 6 have similar TOC, porosity, and saturation average values; however, LF 6 displays a

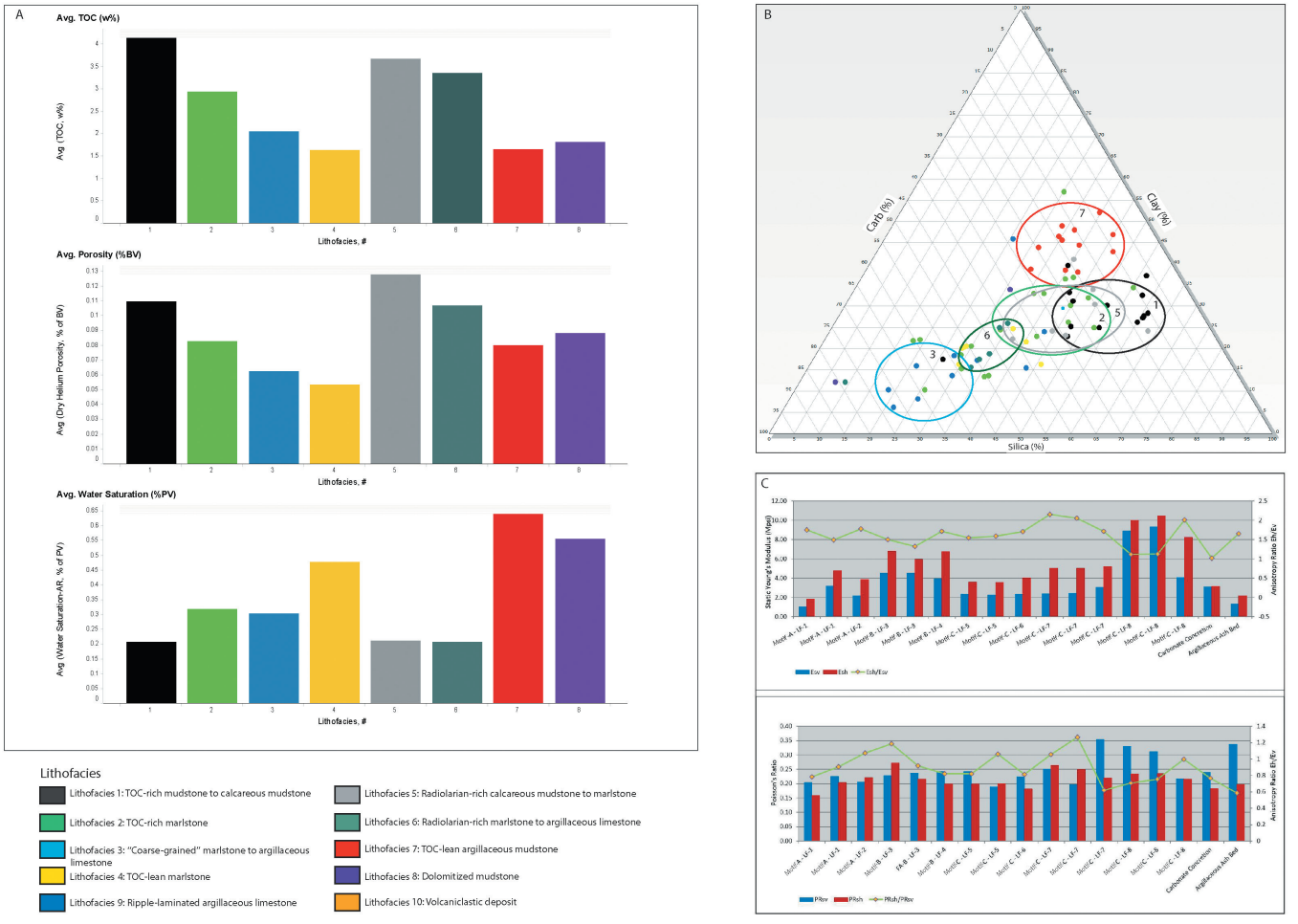

Figure 13. (A) Lithofacies plotted against TOC, porosity, and water saturation. (B) XRD analyses of core samples plotted in a ternary diagram silica–carbonate–clay and grouped by lithofacies (compare colors and numbers with [A]). (C) Lithofacies plotted against Poisson's ratio (above) and static Young's modulus (below); both plots show Anisotropy Ratio (green line), PR_{sv} (blue histograms), and PR_{sh} (red histograms).

mineralogical composition affected by intense early diagenesis that replaced the siliceous radiolarians with calcite and hence presenting XRD values of carbonate as high as 60% (versus 10%–40% in LF 5). LF 7 shows low carbonate content (< 30 %) and high clay content (55%–70%) related to detrital fine-grained siliciclastic sediment deposited in the slope of prograding clinoforms (Motif C). LF 8 represents a diagenetic alteration of LF 7 and is characterized by the presence of dolomite.

Young's Modulus and Poisson's Ratio

Geomechanical properties are a key component in the evaluation of organic-rich mudstone reservoirs as their development requires hydraulic fracturing. Rock stiffness and stress can be evaluated by Young's modulus (YM) and Poisson's ratio (PR) triaxial test lab analysis (Figure 13C). These two parameters greatly control fracture initiation and growth, hydraulic fracture barriers/baffles, fracture heights, near-wellbore conductivity, and proppant embedment (see Varela et al., 2020, this Memoir). In this section we focus on geomechanics from a sedimentological perspective explaining the concepts of homogeneity, heterogeneity, isotropy, and anisotropy of lithofacies. Homogeneous lithofacies display uniform mineral composition, texture, and fabric. Heterogeneous lithofacies are distinctly nonuniform in one of the three mentioned characteristics. Isotropy implies identical physical and mechanical properties of the rock in all directions; anisotropy implies different properties along different directions. The YM represents a proxy to understand rock stiffness and the resultant heterogeneity of a vertical stack of lithofacies.

Where the clinoform presents low-angle foresets (typical of the older sequences), the bottomset (Motif A) is dominated by LF 1, which shows low

YM values varying according to TOC content, abundance of carbonate grains, and diagenetic history. This bottomset also presents numerous argillaceous ash beds (with low YM values and high PR values) and carbonate concretions (with YM anisotropic ratio of 1). Reservoir zones characterized by Motif B are composed by an alternation of carbonate-rich (LF 3) and carbonate-poor lithofacies (LF 2), as also tracked by differences in YM; thus, these intervals show several interfaces with strong geomechanical contrasts. The bottomset and lower foreset of steep clinoforms (motifs A and C) also show an alternation of carbonate-rich and carbonate-poor lithofacies (LF 5 and 6); however, this heterogeneity is not observed in the geomechanical properties, as both lithofacies have very similar values of YM and PR. The main differences in the rocks of clinoforms with changing steepness is that carbonate content within the low-angle foresets is mainly detrital, whereas the carbonate in high-angle foresets is mainly diagenetic. In this latter setting, LF 7, very laminated and rich in clay, presents the highest YM anisotropic ratio, and LF 8 presents the highest YM values.

Landing Zones

Vertical lithological heterogeneity is the most important factor for geomechanics because it can hamper and disrupt the growth of the induced fracture: the lesser the vertical heterogeneity, the easier the fracture growth and the better the landing zone to access the hydrocarbon stored. Within stratigraphic units having similar vertical heterogeneity, the geomechanical contrast (expressed by the YM and PR values) is key. An example of low geomechanical contrast is represented by the alternation of LF 5 and LF 6 in the bottomsets of the younger clinoforms (Unit 4); although LF 5 and LF 6 show different mineralogy in XRD, they present very similar YM values. Instead, within the bottomsets of Unit 1, the high geomechanical contrast is given by the alternation of LF 1, 2, 10, and 12, which shows higher magnitude change of YM values, specially where ash beds (LF 10) and calcareous concretions (LF 12) are in contact. The highest geomechanical contrast is represented by the alternation of LF 1 and 2 and LF 3 and 10, typical of Motif B deposited within the lower and middle foresets of the older clinoforms (Unit 1 to 2).

In general, wells landed in the bottomset have been the best performers so far, given the high hydrocarbon resource density within this depositional sector. However, their estimated ultimate recovery (EUR) varies depending on the specific landing zone window, typically 5–10 m [~15–30 ft] thick.

Within the bottomsets of Unit 1, it is important to avoid, or reduce to a minimum, the presence of calcareous concretions (LF12) and ash beds (LF 10) and place the wells far enough (15–20 m [~50–70 ft]) from potential fracture containment beds (e.g., Tordillo, Motif B, and Motif C). This is the case for wells landed in Motif A of Unit 1 within the landing zone window between 3100 and 3110 m (10,170–10,200 ft) (Figure 4) that resulted in very good performance.

Within the bottomsets of Unit 4, the YM contrast between alternating lithofacies (LF 5 and 6) is low, and the stronger deterrents of fracture growth are the bed-parallel calcite-filled veins (also known as "beef"). In fact, concretions and ash beds are not as common as in Unit 1. Therefore, as heterogeneity is not a major concern, the selection of the landing zone window should maximize the vertical access to hydrocarbon. For example, wells landed in Motif A of Unit 4 within the landing zone window between 3110 and 3120 m (10,170–10,230 ft) show a very good performance because porosity is the highest and there is enough thickness underneath the Motif C, characterized by low bulk-volume hydrocarbon content.

Within the foresets of Units 1 and 2, wells landed in Motif B have had execution challenges (casing constrictions) and results have been mixed, underperforming those of Motif A, because of the presence of recurrent intercalations of LF 1, 2 ,3, 9, and 10 (high vertical heterogeneity) and lower hydrocarbon densities.

The geomechanical heterogeneity, the preservation of high TOC, and the porosity of the Vaca Muerta rocks, today saturated in hydrocarbons, are a function of the sedimentary processes that governed the deposition and diagenesis of those lithologies. Understanding these sedimentary processes enables a more accurate prediction of the lithological variability away from the control points, both geographically and stratigraphically. Specifically, the prediction of the stacking patterns in the bottomset and distal foreset is of paramount importance in the landing zone decisions, including the opportunity to co-develop two or more landing zones in the same depositional sector.

Integration of porosity, TOC, and lithology in the bottomsets

Porosity and TOC follow a similar trend in all depositional sectors and in all sequences. Where TOC drops, porosity drops, and vice versa (Figure 14A). The trends are persistent along the entire length of the cores (tens of meters) and follow even local minimal perturbations (less than 1 m [3 ft]); for example, thin

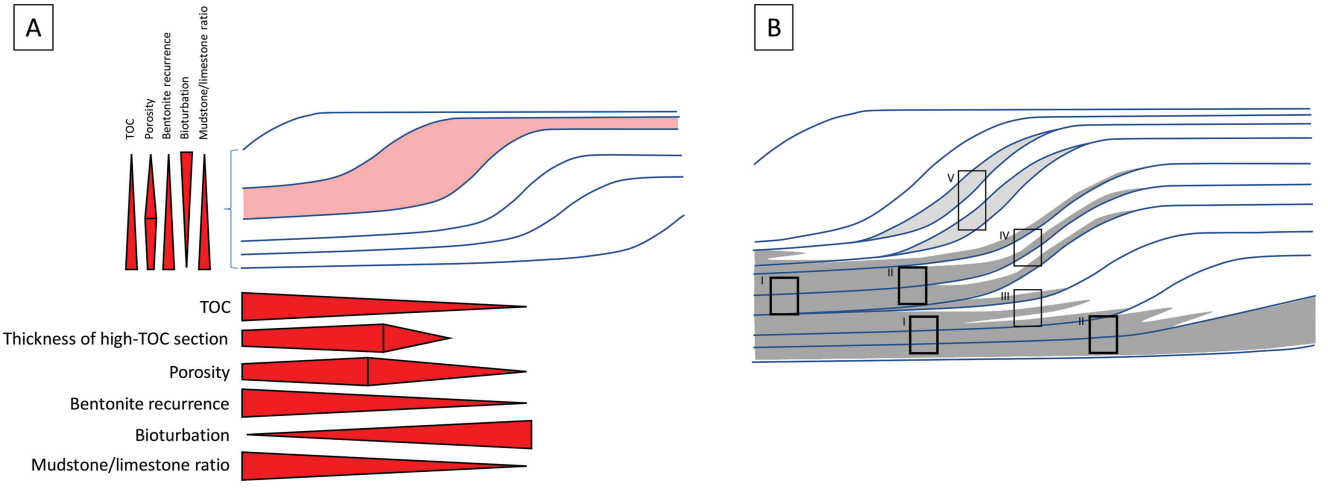

Figure 14. A: Conceptual sketch generalizing trends of independent proxies in the bottomsets and foresets of the Vaca Muerta–Quintuco system (data mainly derived from northern area of the Neuquén Basin). Horizontal trends are related to the shaded unit. Vertical trends are related to the left end of the prograding clinoform. B: Current play concept consisting in landing the horizontal wells in the proximal bottomsets (I) and lower foresets (II), sectors with the best reservoir characteristics. Further play concepts to be proved include: thin carrier beds within high-TOC intervals in the lower foresets (III), tight reservoirs interbedded with transgressive high-TOC intervals in the middle foresets (IV), and stacking of specific foresets with good reservoir characteristics (V).

beds with low TOC correspond to drops in porosity. This observation helps extrapolate the linear relationship between porosity and TOC and to apply it to the cuttings, where porosity and TOC cannot be measured in the same sample. Generally, the TOC is higher (up to 10%) and more broadly distributed in the Jurassic units (Units 1 and 2) than in the Cretaceous units (up to 8%, Units 3–6) (Figure 3). The units with higher TOC also present the highest frequency of ash beds, which are considered "soft rocks" with high stress. The highest frequency of ash beds in the bottomsets is related to the basinward decrease of (1) bioturbation, (2) energetic sedimentary processes, and (3) sediment accumulation rate.

The TOC, porosity, and ash bed trends suggest that the depositional sector with higher hydrocarbon potential is in the proximal bottomset and lower foresets, where porosity shows an optimum with values higher than 14%, and TOC, although not in its optimum sector, registers values around 5% (Figure 14A). The lithology of the proximal bottomset shows (1) a high frequency of subcentimeter ash beds but not as high as in the distal bottomset, where ash beds occur every 18 cm (7 in.) (Minisini, 2017); (2) a high frequency of mudstone–limestone alternations (a 5–20 cm [2–8 in.] limestone bed every 1 m [3 ft]), which is higher than in the distal bottomset (a 5–20 cm [2–8 in.] limestone bed every 3 m [10 ft]), where some limestones appear as elongated concretions. More in specific and at a finer scale, within the proximal bottomset, the highest porosity, the highest TOC, and the lowest water saturation occur in the mudstone lithologies (e.g., LF 1).

The origin and preservation of high porosity that created the extraordinary storage capacity in the Vaca Muerta result from a combination of 1) the original composition of the sediment (pellets with intraparticle pores; organic matter fueling redox reactions and creating dissolution; feldspars dissolving and creating more storage capacity), 2) the sedimentary processes (bottom currents and gravity flows delivering siliciclastic, volcaniclastic, and reworked calcareous bioclastic grains, and fall out of bioclastic material), 3) seafloor and water column chemistry (temporary pulses of anoxia and reductive conditions) triggering early diagenesis (from the metastable organic matter and volcaniclastic material), 4) reduced compaction related to early cementation (as highlighted by the carbonate concretions). The presence of early cement and dissolution fabrics indicates that significant volumes of fluid flowed through these rocks, regardless of their low permeability, hence affecting their pore infill history.

Sedimentology and hydrocarbon production

Hydrocarbon production from the Vaca Muerta Formation is made publicly available by the Provincia de Neuquén, although landing zones are undisclosed.

Those data allow the creation of a "bubble map" of peak production from horizontal wells (map in Figure 15 shows wells with lateral drain longer than 1500 m). Because TOC is a key parameter in the self-sourced unconventional plays, the "bubble map" is overlain to the thickness of the organic-rich section (TOC > 2%) of each unit (Units 1–5) to analyze their relationship. The depocenters of the organic-rich sections occur along the proximal bottomsets and lower foresets, which represent the optimum landing zones, as previously described (Figure 14B). Although uncertain, it is assumed that most horizontal wells targeted proximal bottomsets and lower foresets.

While migrating toward northwest, the organic-rich section of each unit partially overlaps the organic-rich section of the previous unit; however, the organic-rich sections decrease in extent and thickness with time, and by the time of Unit 4, they do not overlap anymore (Figure 15). Unit 5 is an exception, as it moves southward overriding the Quintuco Formation (Figure 2), but its TOC is the lowest and water saturation the highest among the units (see figure 12 of Ortiz et al., 2020, this Memoir).

The map overlying the thickness of high-TOC stratigraphic sections and the peak hydrocarbon production allows us to infer that the most productive wells are located in the depocenters of the high-TOC sections and the least productive wells are located in areas with thin high-TOC sections. Furthermore, the distribution of the wells in production seems to be controlled by the Añelo axes of subsidence (see structural features in figure 4 of Dominguez et al., 2020a, this Memoir). However, correlation does not imply causation; therefore further investigations on non-technical risks and other key production factors are needed (e.g., stress regime, natural fractures, volcanic intrusions, etc.) before claiming that the depocenters of the high-TOC sections, and areas of subsidence, control or affect the production and sweet spots.

PLAY CONCEPTS

The concept of hydraulic fracturing in the Vaca Muerta self-sourced unconventional play was proved by means of vertical wells in 2011. The initial development concept was that the Vaca Muerta extraordinary pay thickness was enough to produce economically through vertical wells with multiple fracture stages (e.g., 250 m of vertical target completed with five fracture stages per well). However, in 2012, the introduction of multi-well pads dramatically scaled up the drilling technology threshold, and their results kicked off a new concept of hydraulic fracturing, now based on multiple horizontal wells (generally three or four) drilled from the same surface pad, thus enabling simultaneous operations, minimizing the environmental footprint, and reducing the number of rigs needed (Minisini et al., 2020, this Memoir).

The current play concept consists in landing the horizontal wells in the proximal bottomsets and lower foresets, sectors with higher hydrocarbon storage potential and easier fracture growth (i.e., larger stimulated rock volume). The rocks in these sectors show the best reservoir characteristics (TOC > 2%, av. 5%; porosity > 8%, av. 11%–12%; clay <40%, av. 10–20%, water saturation <50%, av. 20%), the most adequate geomechanical properties (YM < 4 Mpsi, low Poisson Ratio ~0.25, and homogeneous rock units exhibiting interfaces with weak geomechanical contrasts) and a thick vertical stack of lithofacies with the aforementioned characteristics (av. 30–40 m) (Figure 14A and Figure 14B, windows I and II). Although the distal bottomsets register the highest TOC, they are not a preferred landing zone in the active areas because (with respect to proximal bottomsets) porosity is lower, clay is higher, sub-centimeter ash beds have the highest recurrence, concretions and sills are more numerous, and landing zones are thinner (Figure 14A). With this concept in mind, at least two landing zones have been fully de-risked and are producing in "factory mode" in the development phase (lower Unit 1 and lower Unit 2 -aka Cocina and Organico), and other five-six landing zones have been tested with production logging tool (PLT) data showing encouraging results (Figure 5). All current successful landing zones are in the Embayment area where hydrocarbon potential is the highest and wells produce high-quality low-sulfur oils and gas condensates (see figure 1 in Brisson et al., 2020, this Memoir).

In the future, a further play concept may be tested in the foresets, where the number of landing wells has increased since 2019. As evidenced by subtle variations in various seismic stacking patterns, the clinoforms did not prograde uniformly, and advanced (as a delta) with discrete steps, recording foresets with variable direction, extent, geometry, lithofacies, and aggradational component (see Dominguez et al., 2020b, this Memoir). Within this variability, some foresets should be avoided (i.e., the ones with coarse bottom-current deposits, see Reijenstein et al., 2020, this Memoir), but some foresets with appropriate reservoir characteristics and thickness do exist, and represent promising prospects. This new play concept in the foresets consists of a stacking of thin foresets with good reservoir characteristics interbedded with thicker foresets with bad reservoir characteristics, creating a

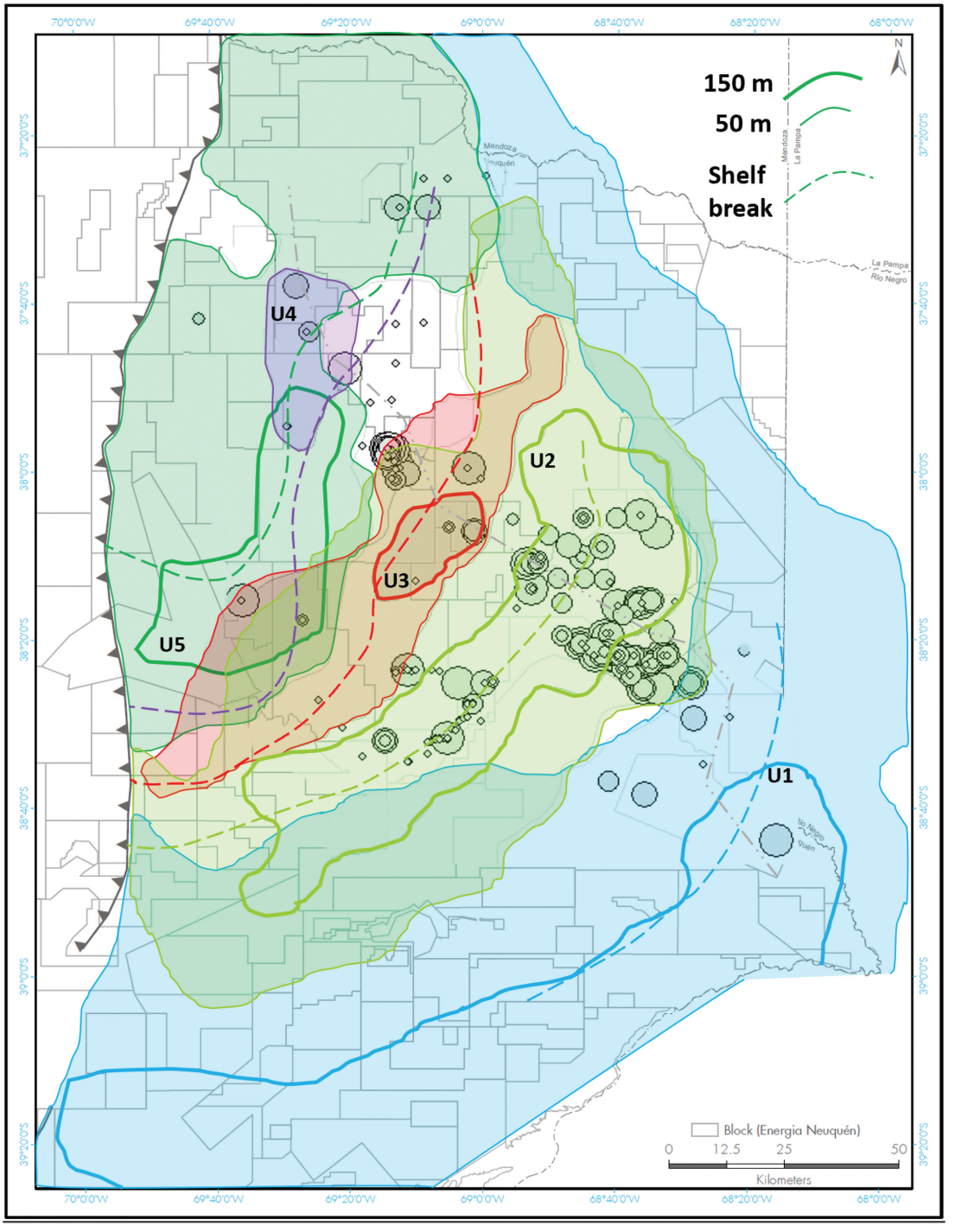

Figure 15. Map overlying peak hydrocarbon production per well and thickness of organic-rich stratigraphic sections. Bubbles represent production from horizontal wells with lateral drain longer than 1500 m; the five bubble sizes represent 200–400–600–800–1,000 boe (note that the landing zone of the productive wells is not publicly declared). The contours represent 50 and 150 m [~160 and 500 ft] thickness of the organic-rich sections (TOC > 2%) for five units of the Vaca Muerta-Quintuco system (U1 to U5, see Figure 2).

hybrid unconventional play, similar to the Niobrara play in the DJ Basin, the Bazhenov play in Russia, the Wolfberry and Bone Spring plays in the Permian Basin (Figure 14B, windows III and V). Another option consists of transgressive units with good reservoir characteristics, typically deposited in the bottomsets, and cyclically depositing in the foresets (see figure 10 of Dominguez et al., 2020b, this Memoir; figure 15 of Reijenstein et al., 2020, this Memoir). The interbedding of 1) muddy, high-TOC, transgressive units, climbing the clinoform from the bottomsets during sea level rise, and 2) coarse and lean foresets enhances the idea of a hybrid play where source rocks and tight reservoirs are interbedded (Figure 14B, window IV). Furthermore, in the future, exploration may move beyond the Embayment area into the structural highs, in the fold-and-thrust belt, in sectors affected by igneous intrusions, and in areas where the Vaca Muerta is deeply buried.

CONCLUSIONS

The studies devoted to the sedimentology and stratigraphy of a self-sourced unconventional play help its evaluation and optimization when linked with the petrophysical and geomechanical parameters of the rocks because they define the potential volume of hydrocarbons and the capability to fracture the rock. Linking sedimentology and stratigraphy with petrophysics and geomechanics helps identify the best areas to land horizontal wells and predict high recovery of resources (Figure 1).

The Vaca Muerta–Quintuco system is a mixed carbonate–siliciclastic prograding clinoform. The Vaca Muerta Formation corresponds to the bottomsets and foresets of the clinoforms, and the Quintuco Formation corresponds to the topsets (Figure 2).

The triggers producing the progradation of the clinoform are (1) the increase in sediment input (controlled by climate) and (2) the decrease in accommodation space (controlled by local tectonic movements). The sediment in the clinoform is deposited as follows:

- Benthic biogenic carbonate (skeletal grains and fecal pellets) originated in the shallow seafloor (topset); planktonic biogenic carbonate (foraminifera) and quartz (radiolaria) originated in the water column above the entire clinoform; siliciclastic and volcaniclastic material entered the basin by wind and rivers; and intrabasinal muddy rip-up clasts were created by bottom currents and muddy turbidity currents.
- Part of the sediment in the bottomset was delivered directly by extrabasinal hyperpycnal flows (especially in the south, Picún Leufú area), but most of it was first deposited in the topset and then reworked basinward by tides and bottom currents, and then captured by gyres and redistributed both along and across slope. When the activity of currents was scarce, deposition by fallout was more common. Once settled, the sediment was overprinted by early diagenesis: clays derived from the volcaniclastic material, quartz from radiolaria, and micrite from the abundant carbonate material.
- The first clinoforms (Units 1 and 2) represent the low-angle ramp of a carbonate system developed in shallow water during sea level rise. The successive clinoforms (Units 3–6) recorded higher siliciclastic input, which filled the accommodation space, hence allowing enhanced hydrodynamic processes (waves, currents, and gravity flows) that created steeper foresets.
- The steeper foresets ignited gravity flows and allowed stronger bottom currents. When a distinguishable shelf break was created, current activity was enhanced triggering hydrodynamic accumulations (banks, shoals) and in situ organic biohermal buildups in the distal topset, which in turn formed an incipient lithified margin (Unit 3).

The bottomsets and the lower foresets of the clinoforms are characterized by a high density of hydrocarbon resources. The largest bulk-volume hydrocarbon is associated with organic-rich mudstone and marlstone (lithofacies 1 and 2 in Figure 4, Table 1) that deposited during recurrent periods of transgressions, characterized by low sediment accumulation rate, basinwide suboxia–anoxia, and high bio-productivity.

The recurrent transgressions created a stacking of bottomsets and lower foresets with a high density of hydrocarbon resources, generating a sedimentary wedge that thickened basinward with time, during the entire Vaca Muerta–Quintuco system that lasted approximately 11 My (Figures 2, 3, 14).

The current play concept consists in landing the horizontal wells in the proximal bottomsets and lower foresets of the clinoform, where rocks show the best reservoir characteristics (TOC 5%; porosity 12%; clay 10–20%, water saturation 20%), the most adequate geomechanical properties (homogeneous rock with Young's Modulus <4 Mpsi, low Poisson Ratio ~0.25, and homogeneous rock units exhibiting interfaces with weak geomechanical contrasts) and a thick vertical stack of lithofacies with the aforementioned

characteristics (30–40 m) (Figure 14). The preferred areas for high hydrocarbon production seem to be related to the depocenters of the high-TOC sections, in the Embayment area (Figure 15). In the future, operations may move beyond this area exploring the structural highs, the fold-and-thrust belt, the areas affected by igneous intrusions, and those where the Vaca Muerta is deeply buried.

ACKNOWLEDGMENTS

The authors thank the reviewers Carlos Arregui and Manuel Fantín for their help in integrating a manuscript that, although benefited from a rich data set and multiple points of view, struggled with the conundrum on how to homogenize them. The authors thank their companies for allowing publication. DM thanks Bob Fryklund for helping preparing Figure 15 and for the time shared to connect the evolution of a complex sedimentological system with the practical understanding of the variable hydrocarbon production from rocks apparently under self-similar conditions. DM also thanks Hernan Reijenstein for the passionate discussions around the "play concepts".

REFERENCES CITED

Aigner, T., and H. E. Reineck, 1982, Proximality trends in modern storm sands from the Helgoland Bight (North Sea) and their implication for basin analysis: Senkenb. Maritima, v. 14, p. 183–215.

Allen, J. R. L., 1969, Erosional current marks of weakly cohesive mud beds: Journal of Sedimentary Research, v. 39, no. 2, p. 607–623.

Aplin, A. C., and J. H. Macquaker, 2011, Mudstone diversity. Origin and implications for source, seal, and reservoir properties in petroleum systems: AAPG Bulletin, v. 95, no. 12, p. 2031–2059.

Arregui, C., 2014, Ciclos deposicionales de las Fms Quintuco y Vaca Muerta: génesis y evolución: 9° Congreso de Exploración y Desarrollo de Hidrocarburos, Mendoza, Argentina, 3–7 November, p. 189–207.

Baudin, F., J. R. Disnar, P. Martinez, and B. Dennielou, 2010, Distribution of the organic matter in the channel-levees systems of the Congo mud-rich deep-sea fan (West Africa). Implication for deep offshore petroleum source rocks and global carbon cycle: Marine and Petroleum Geology, v. 27, no. 5, p. 995–1010.

Baudin, F., P. Martinez, B. Dennielou, K. Charlier, T. Marsset, L. Droz, and C. Rabouille, 2017a, Organic carbon accumulation in modern sediments of the Angola basin influenced by the Congo deep sea fan: Deep Sea Research Part II: Topical Studies in Oceanography, v. 142 (August), p. 64–74.

Baudin, F., E. Stetten, J. Schnyder, K. Charlier, P. Martinez, B. Dennielou, and L. Droz, 2017b, Origin and distribution of the organic matter in the distal lobe of the Congo deep-sea fan—A rock-eval survey: Deep-Sea Research Part II: Topical Studies in Oceanography, v. 142, p. 75–90.

Betzler, C., S. Lindhorst, G. P. Eberli, T. Lüdmann, J. Möbius, J. Ludwig, I. Schutter, M. Wunsch, J. J. G. Reijmer, and C. Hübscher, 2014, Periplatform drift: The combined result of contour current and off-bank transport along carbonate platforms: Geology, v. 42, p. 871–874.

Bhattacharya, J. P., and J. A. MacEachern, 2009, Hyperpycnal rivers and prodeltaic shelves in the Cretaceous seaway of North America: Journal of Sedimentary Research, v. 79, no. 4, p. 184–209.

Biscara, L., T. Mulder, P. Martinez, F. Baudin, H. Etcheber, J. M. Jouanneau, and T. Garlan, 2011, Transport of terrestrial organic matter in the Ogooué deep sea turbidite system (Gabon): Marine and Petroleum Geology, v. 28, no. 5, p. 1061–1072.

Blanpied, C., and D. J. Stanley, 1981, Uniform mud (unifite) deposition in the Hellenic Trench, Eastern Mediterranean: Smithsonian Contributions to the Marine Sciences, no. 13, 40 p. https://repository.si.edu/bitstream/handle/10088/22483/SCMS-0013.pdf?sequence=1&isAllowed=y.

Boggs, S. Jr., 2001, The oceanic (deep-water) environment, *in* S. Boggs Jr., ed., Principles of sedimentology and stratigraphy, 3rd ed.: Upper Saddle River, NJ, Prentice-Hall, p. 349–364.

Bohacs, K. M., O. R. Lazar, and T. M. Demko, 2014, Parasequence types in shelfal mudstone strata-Quantitative observations of lithofacies and stacking patterns, and conceptual link to modern depositional regimes: Geology, v. 42, no. 2, p. 131–134.

Brisson, I. E., M. E. Fasola, and H. J. Villar, 2020, Organic geochemical patterns of the Vaca Muerta Formation, *in* D. Minisini, M. Fantín, I. Lanusse Noguera, and H. A. Leanza, eds., Integrated geology of unconventionals: The case of the Vaca Muerta play, Argentina: AAPG Memoir 121, p. 297–328.

Clifton, H. E., 1957, The carbonate concretions of the Ohio Shale: The Ohio Journal of Science, v. 57, p. 114–129.

Denommee, K. C., S. J. Bentley, D. Harazim, and J. H. Macquaker, 2016, Hydrodynamic controls on muddy sedimentary-fabric development on the Southwest Louisiana subaqueous delta: Marine Geology, v. 382, p. 162–175.

Desjardins, P., M. Fantín, F. González Tomassini, H. Reijenstein, F. Sattler, F. Domínguez, D. Kietzmann, H. Leanza, A. Bande, S. Benoit, M. Borgnia, F. Vittore, T. Simo and D. Minisini, 2018, Chapter 2: Regional Seismic Stratigraphy, *in* G. González, M. D. Vallejo, D. Kietzmann, D. Marchal, P. Desjardins, F. González Tomassini, L. Gómez Rivarola, and R. F. Domínguez, eds., Regional cross section of the Vaca Muerta Formation. Integration of seismic, well logs, cores, and outcrops: Special Publication of Instituto Argentino del Petróleo y del Gas (IAPG), Buenos Aires, Argentina, p. 5–22.

Desjardins, P., and H. Aguirre, 2018, Chapter 7: Sierras Blancas, *in* G. González, M. D. Vallejo, D. Kietzmann, D. Marchal, P. Desjardins, F. González Tomassini, L. Gómez Rivarola, and R. F. Domínguez, eds., Regional cross section of the Vaca Muerta Formation. Integration of seismic, well logs, cores, and outcrops: Special Publication of Instituto Argentino del Petróleo y del Gas (IAPG), Buenos Aires, Argentina, p. 71–82.

Domínguez, R. F., C. Bernhardt, F. González Tomassini, M. Fantín, and M. Di Benedetto, 2018, Variaciones paleogeográficas de las unidades ricas en materia orgánica de la formación Vaca Muerta en el engolfamiento Neuquino, 10° Congreso de Exploración y Desarrollo de Hidrocarburos, 5–9 November, Mendoza, Argentina, contribution 1685.

Domínguez, R. F., O. Catuneanu, H. M. Reijenstein, R. Notta, and H. W. Posamentier, 2020a, Sequence stratigraphy and the three-dimensional distribution of organic-rich units, *in* D. Minisini, M. Fantín, I. Lanusse Noguera, and H. A. Leanza, eds., Integrated geology of unconventionals: The case of the Vaca Muerta play, Argentina: AAPG Memoir 121, p. 163–200.

Domínguez, R. F., H. A. Leanza, M. Fantín, D. Marchal, and E. Cristallini, 2020b, Basin configuration during the Vaca Muerta times, *in* D. Minisini, M. Fantín, I. Lanusse Noguera, and H. A. Leanza, eds., Integrated geology of unconventionals: The case of the Vaca Muerta play, Argentina: AAPG Memoir 121, p. 141–162.

Dong, J., S. Zhang, G. Jiang, Q. Zhao, H. Li, X. Shi, and J. Liu, 2008, Early diagenetic growth of carbonate concretions in the upper Doushantuo Formation in South China and their significance for the assessment of hydrocarbon source rock: Science in China Series D: Earth Sciences, v. 51, no. 9, p. 1330–1339.

Eberli, G. P., and C. Betzler, 2019, Characteristics of modern carbonate Contourite drifts: Sedimentology, v. 66, p. 1163–1191, DOI: 10.1111/sed.12584.

Eberli, G. P., R. J. Weger, M. Tenaglia, L. Rueda, L. Rodriguez Blanco, M. Zeller, D. F. McNeill, S. Murray, and P. K. Swart, 2017, The unconventional play in the Neuquén Basin, Argentina – Insights from the outcrop for the subsurface: Unconventional Resources Technology Conference, Extended Abstract, URTeC 2687581, Austin, Texas, July 24–26, p. 1–12.

Einsele, G., R. Overbeck, H. U. Schwarz, and G. Unsöld, 1974, Mass physical properties, sliding and erodibility of experimentally deposited and differentially consolidated clayey muds: Sedimentology, v. 21, no. 3, p. 339–372.

Enos, P., and L. H. Sawatsky, 1981, Pore networks in Holocene carbonate sediments: Journal of Sedimentary Research, v. 51, no. 3, p. 961–985.

Estrada, S. J., M. F. Raverta, M. de Santa Coloma, J. P. Torres, and S. Galeazzi, 2020, Pilot phase of the Aguada Pichana Este Block, gas window, *in* D. Minisini, M. Fantín, I. Lanusse Noguera, and H. A. Leanza, eds., Integrated geology of unconventionals: The case of the Vaca Muerta play, Argentina: AAPG Memoir 121, p. 497–514.

Galeazzi, S., G. González, M. Santiago, D. García, L. Maschio, R. González, and J. Ramírez Martínez, 2014, Simposio de Recursos No Convencionales: Ampliando el Horizonte Energético, 1ª edición: Instituto Argentino del Petróleo y Gas (IAPG), Buenos Aires, Argentina, 904 p.

Goldhammer, R. K., 1997, Compaction and decompaction algorithms for sedimentary carbonates: Journal of Sedimentary Research, v. 67, no. 1, p. 26–35.

Gómez Rivarola, L., and M. Borgnia, 2018, Chapter 13: San Roque, *in* G. González, D. Vallejo, P. Desjardins, F. Gonzalez-Tomassini, D. Kietzmann, L. Rivarola, and F. Domínguez, eds., Regional cross section of the Vaca Muerta Formation. Integration of seismic, well logs, cores and outcrops: Special Publication Instituto Argentino de Petróleo y el Gas (IAPG), Buenos Aires, Argentina, p. 143–153.

González, G., M. D. Vallejo, D. Kietzmann, D. Marchal, P. Desjardins, F. González Tomassini, L. Gómez Rivarola, and R. F. Domínguez, 2018, eds., Regional cross section of the Vaca Muerta Formation. Integration of seismic, well logs, cores, and outcrops. Special Publication of Instituto Argentino del Petróleo y del Gas (IAPG), Buenos Aires, Argentina, 249 p.

Kietzmann, D. A., and R. M. Palma, 2011, Las tempestitas peloidales de la Formación Vaca Muerta (Tithoniano–Valanginiano) en el sector surmendocino de la Cuenca Neuquina, Argentina: Latin American Journal of Sedimentology and Basin Analysis, v. 18, p. 121–149.

Kietzmann, D. A., and R. M. Palma, 2014, Early Cretaceous crustacean microcoprolites from Sierra de la Cara Cura, Neuquén Basin, Argentina: Taphonomy, environmental distribution, and stratigraphic correlation: Cretaceous Research, v. 49, p. 214–228.

Kietzmann, D. A., A. L. Ambrosio, J. Suriano, M. S. Alonso, F. G. Tomassini, G. Depine, and D. Repol, 2016, The Vaca Muerta–Quintuco system (Tithonian–Valanginian) in the Neuquén Basin, Argentina: A view from the outcrops in the Chos Malal fold and thrust belt: AAPG Bulletin, v. 100, no. 5, p. 743–771.

Kietzmann, D. A., J. Martín-Chivelet, R. M. Palma, J. López-Gómez, M. Lescano, and A. Concheyro, 2011, Evidence of precessional and eccentricity orbital cycles in a Tithonian source rock: The mid-outer carbonate ramp of the Vaca Muerta Formation, northern Neuquén Basin, Argentina: AAPG Bulletin, v. 95, p. 1459–1474.

Kietzmann, D. A., R. M. Palma, A. C. Riccardi, J. Martín-Chiveler, and J. López-Gómez, 2014, Sedimentology and sequence stratigraphy of a Tithonian - Valanginian carbonate ramp (Vaca Muerta Formation): A misunderstood exceptional source rock in the Southern Mendoza area of the Neuquén Basin, Argentina: Sedimentary Geology, v. 302, p. 64–86.

Kietzmann, D. A., F. González Tomassini, and T. Smith, 2020, Grain association, petrography, and lithofacies, *in* D. Minisini, M. Fantín, I. Lanusse Noguera, and H. A. Leanza, eds., Integrated geology of unconventionals: The case of the Vaca Muerta play, Argentina: AAPG Memoir 121, p. 267–296.

Könitzer, S. F., S. J. Davies, M. H. Stephenson, and M. J. Leng, 2014, Depositional controls on mudstone lithofacies in a basinal setting: Implications for the delivery of sedimen-

tary organic matter: Journal of Sedimentary Research, v. 84, no. 3, p. 198–214.

Lash, G. G., 2016, Hyperpycnal transport of carbonaceous sediment–example from the Upper Devonian Rhinestreet Shale, western New York, USA: Palaeogeography, Palaeoclimatology, Palaeoecology, v. 459, p. 29–43, DOI: 10.1016/j.palaeo.2016.06.035.

Lash, G. G., and D. Blood, 2004, Geochemical and textural evidence for early (shallow) diagenetic growth of stratigraphically confined carbonate concretions, Upper Devonian Rhinestreet black shale, western New York: Chemical Geology, v. 206, no. 3, p. 407–424.

Lazar, R., K. M. Bohacs, J. Schieber, J. Macquaker, and T. Demko, 2015, Mudstone Primer: Lithofacies variations, diagnostic criteria, and sedimentologic-stratigraphic implications at lamina to bedset scale: Oklahoma, Society for Sedimentary Geology, 204 p.

Leanza, H. A., D. A. Kietzmann, M. P. Iglesia Llanos, and M. Kohan Martínez, 2020, Stratigraphic context: Cyclostratigraphy, magnetostratigraphy, and seismic stratigraphy, *in* D. Minisini, M. Fantín, I. Lanusse Noguera, and H. A. Leanza, eds., Integrated geology of unconventionals: The case of the Vaca Muerta play, Argentina: AAPG Memoir 121, p. 39–60.

Leanza, H. A., H. G. Marchese, and J. C. Riggi, 1977, Estratigrafía del Grupo Mendoza con especial referencia a la Formación Vaca Muerta entre los Paralelos 35° y 40° ls Cuenca Neuquina-Mendocina: Revista de la Asociación Geológica Argentina, v. 32, no. 3, p. 190–208.

Legarreta, L., and M. A. Uliana, 1991, Jurassic-Cretaceous marine oscillations and geometry of backarc basin fill, central Argentine Andes, *in* D. I. MacDonald, ed., Sedimentation, tectonics and eustasy: Sea level changes at active plate margins: Oxford, International Association of Sedimentologists, Special Publication 12, p. 429–450.

Legarreta, L., E. Kozlowski, and A. Boll, 1981, Esquema estratigráfico y distribución de facies del Grupo Mendoza en el ámbito surmendocino de la cuenca Neuquina, *in* 8° Congreso Geológico Argentino, Actas 3, San Luis, Argentina, p. 389–409.

Macquaker, J. H. S., and R. L. Gawthorpe, 1993, Mudstone lithofacies in the Kimmeridge Clay Formation, Wessex Basin, southern England: Implications for the origin and controls of the distribution of mudstones: Journal of Sedimentary Research, v. 63, no. 6, p. 1129–1143.

Macquaker, J. H., S. J. Bentley, and K. M. Bohacs, 2010, Wave-enhanced sediment-gravity flows and mud dispersal across continental shelves: Reappraising sediment transport processes operating in ancient mudstone successions: Geology, v. 38, p. 947–950, DOI: 10.1130/G31093.1.

Macquaker, J. H., K. G. Taylor, and R. L. Gawthorpe, 2007, High-resolution facies analyses of mudstones: Implications for paleoenvironmental and sequence stratigraphic interpretations of offshore ancient mud-dominated successions: Journal of Sedimentary Research, v. 77, no. 4, p. 324–339.

Macquaker, J. H., Taylor, K. G., Keller, M. and Polya, D., 2014, Compositional controls on early diagenetic pathways in fine-grained sedimentary rocks: Implications for predicting unconventional reservoir attributes of mudstones, AAPG bulletin, 98(3), p. 587–603.

Mángano, M. G., Buatois, L. A., West, R. R., Maples, C. G., 1998, Contrasting behavioral and feeding strategies recorded by tidal-flat bivalve trace fossils from the Upper Carboniferous of eastern Kansas: Palaios, 13, p. 335–351.

Marshall, J. D., and D. Pirrie, 2013, Carbonate concretions—Explained: Geology Today, v. 29, no. 2, p. 53–62.

Mignard, S. L. A., T. Mulder, P. Martinez, K. Charlier, L. Rossignol, and T. Garlan, 2017, Deep-sea terrigenous organic carbon transfer and accumulation: Impact of sea-level variations and sedimentation processes off the Ogooue River (Gabon): Marine and Petroleum Geology, v. 85, p. 35–53.

Minisini D., 2017. Applications of Ash Beds in Petroleum Systems Analysis, AAPG Geological Technical Workshop, Moving toward the prediction of unconventional plays: Lessons learned from tight and shale reservoirs in the Neuquén Basin, Buenos Aires, Argentina, 16–18 November.

Minisini, D., B. Fryklund, F. Gerali, and M. Fantín, 2020, The first economical unconventional play outside North America: Context, history, and "coopetition," *in* D. Minisini, M. Fantín, I. Lanusse Noguera, and H. Leanza, eds., Integrated geology of unconventionals: The case of the Vaca Muerta play, Argentina: AAPG Memoir 121, p. 1–24.

Minisini, D., J. Eldrett, S. C. Bergman, and R. Forkner, 2018, Chronostratigraphic framework and depositional environments in the organic-rich, mudstone-dominated Eagle Ford Group, Texas, USA: Sedimentology, v. 65, no. 5, p. 1520–1557.

Minisini, D., M. Wang, S. C. Bergman, and C. Aiken, 2014, Geological data extraction from lidar 3-D photorealistic models: A case study in an organic-rich mudstone, Eagle Ford Formation, Texas: Geosphere, v. 10, no. 3, p. 610–626.

Mitchum, R. M., and M. A. Uliana, 1985, Seismic stratigraphy of carbonate depositional sequences, Upper Jurassic-Lower Cretaceous, Neuquén Basin, Argentina, *in* O. Berg and D. Woolverton, eds., Seismic stratigraphy, II: An integrated approach to hydrocarbon exploration: AAPG Memoir 39, p. 255–274.

Morettini, E., G. Godino, L. B. Smith, and J. L. Massaferro, 2015, The Vaca Muerta–Quintuco mixed depositional system: New insights from carbon stable isotopes ($\delta^{13}C_{carb}$ and $\delta^{13}C_{org}$) and geochemical data at the Jurassic–Cretaceous boundary (Neuquén Basin, West Argentina), AAPG Search and Discovery article 90216.

Mulder, T., and J. Alexander, 2001, The physical character of subaqueous sedimentary density flows and their deposits: Sedimentology, v. 48, no. 2, p. 269–299.

Mulder, T., J. P. Syvitski, S. Migeon, J. C. Faugeres, and B. Savoye, 2003, Marine hyperpycnal flows: Initiation, behavior and related deposits. A review: Marine and Petroleum Geology, v. 20, no. 6, p. 861–882.

Nakajima, T., 2006, Hyperpycnites deposited 700 km away from river mouths in the Central Japan Sea: Journal of Sedimentary Research, v. 76, no. 1, p. 59–72.

Nielsen, O., D. Curia, P. Pateti, J. Caniggia, A. Ortega, and M. Slinde, 2020, Pilot phase of the Aguada Federal Block, black-oil window, *in* D. Minisini, M. Fantín, I. Lanusse Noguera, and H. A. Leanza, eds., Integrated geology of unconventionals: The case of the Vaca Muerta play, Argentina: AAPG Memoir 121, p. 469–496.

Notta, R., E. Kruijs, V. Jain, G. Diaz-Perez, and H. Mandler, 2020, De-risking the Sierras Blancas and Cruz de Lorena blocks, black-oil window, *in* D. Minisini, M. Fantín, I. Lanusse Noguera, and H. A. Leanza, eds., Integrated geology of unconventionals: The case of the Vaca Muerta play, Argentina: AAPG Memoir 121, p. 445–468.

O'Brien, N. R., and R. M. Slatt, 1990, Argillaceous rock atlas: New York, Springer Science and Business Media, 141 p.

Orchuela, I. A., V. Ploszkiewicz, and R. Viñes, 1981, Reinterpretación estructural de la denominada "Dorsal Neuquina", 8° Congreso Geológico Argentino, Actas v. 3, San Luis, Argentina.

Ortiz, A. C., L. Crousse, C. Bernhardt, D. Vallejo, and L. Mosse, 2020, Reservoir properties: Mineralogy, porosity, and fluid types, *in* D. Minisini, M. Fantín, I. Lanusse Noguera, and H. A. Leanza, eds., Integrated geology of unconventionals: The case of the Vaca Muerta play, Argentina: AAPG Memoir 121, p. 329–350.

Otharán, G., C. Zavala, M. Arcuri, M. Di Meglio, A. Zorzano, D. Marchal, and G. Köhler, 2020, Facies analysis of fine-grained deposits related to muddy underflows. Vaca Muerta Formation (Tithonian-Valanginian), central Neuquen Basin, Argentina: Andean Geology, v. 47/2, p. 384–417.

Otharán, G., C. Zavala, M. Arcuri, D. Marchal, G. Köhler, M. Di Meglio, and A. Zorzano, 2018, The role of fluid mud flows in the accumulation of organic-rich shales. The Upper Jurassic-Lower Cretaceous Vaca Muerta Formation, Neuquén Basin, Argentina, 10° Congreso de Exploración y Desarrollo de Hidrocarburos, 5–9 November, Mendoza, Argentina, p. 61–90.

Paz, M., J. J. Ponce, L. A. Buatois, M. G. Mángano, N. B. Carmona, E. Pereira, and P. R. Desjardins, 2019, Bottomset and foreset sedimentary processes in the mixed carbonate-siliciclastic Upper Jurassic-Lower Cretaceous Vaca Muerta Formation, Picún Leufú Area, Argentina: Sedimentary Geology, v. 389, p. 161–185.

Pettijohn, F. J., 1975, Sedimentary rocks, 3rd ed.: New York, Harper and Row, 628 p.

Pilskaln, C. H., A. C. Neumann, and J. M. Bane, 1989, Periplatform carbonate flux in the northern Bahamas: Deep Sea Research Part A. Oceanographic Research Papers, v. 36, p. 1391–1406.

Plint, A. G., J. H. Macquaker, and B. L. Varban, 2012, Bedload transport of mud across a wide, storm-influenced ramp: Cenomanian–Turonian Kaskapau Formation, western Canada foreland basin: Journal of Sedimentary Research, v. 82, no. 11, p. 801–822.

Pose, F., A. Gangui, and S. Galeazzi, 2014, Estratigrafía secuencial del intervalo Quintuco-Vaca Muerta en el Engolfamiento Neuquino, Cuenca Neuquina, Argentina, *in* 9° Congreso de Exploración y Desarrollo de Hidrocarburos, 3–7 November, Mendoza, Argentina, p. 341–364.

Potter, P. E., J. B. Maynard, and W. A. Pryor, 1980, Sedimentology of shale: New York, Springer Verlag, 303 p.

Potter, P. E., J. B. Maynard, and P. J. Depetris, 2005, Mud and mudstones: Introduction and overview: Alemania, Springer Science y Business Media, 304 p.

Ramos, V. A., M. Naipauer, H. A. Leanza, and M. E. Sigismondi, 2020, An exceptional tectonic setting along the Andean continental margin, *in* D. Minisini, M. Fantín, I. Lanusse Noguera, and H. A. Leanza, eds., Integrated geology of unconventionals: The case of the Vaca Muerta play, Argentina: AAPG Memoir 121, p. 25–38.

Rebesco, M., F. J. Hernández-Molina, D. Van Rooij, and A. Wåhlin, 2014. Contourites and associated sediments controlled by deep-water circulation processes: State-of-the-art and future considerations: Marine Geology, v. 352, p. 111–154.

Reijenstein, H., I. Lanusse, P. Oviedo, D. Licitra, D. Sotelo, F. Vittore, J. Quiroga, and F. González Tomassini, 2017, ¿Deslizamientos en Vaca Muerta? Observaciones e integración de datos sísmicos, pozos y coronas en el yacimiento Loma Campana, Cuenca Neuquina, Argentina: 20° Congreso Geológico Argentino, 7–11 August, San Miguel de Tucumán, Argentina, p. 122–129.

Reijenstein, H. M., H. W. Posamentier, A. Bande, F. A. Lozano, R. F. Domínguez, R. Wilson, O. Catuneanu, and S. Galeazzi 2020, Seismic geomorphology, depositional elements, and clinoform sedimentary processes: Impact on unconventional reservoir prediction, *in* D. Minisini, M. Fantín, I. Lanusse Noguera, and H. A. Leanza, eds., Integrated geology of unconventionals: The case of the Vaca Muerta play, Argentina: AAPG Memoir 121, p. 237–266.

Rodriguez Blanco, L., 2016, Distribution and source of carbonate-rich intervals within the Vaca Muerta-Quintuco mixed system, Neuquén Basin, Argentina: University of Miami, Open Access Theses, 622 p.

Rodriguez Blanco, L., G. P. Eberli, and R. J. Weger, 2017, Distribution and source of carbonate-rich intervals within the Vaca Muerta Formation, *in* 20° Congreso Geológico Argentino, 7–11 August, San Miguel de Tucumán, Argentina, p. 135–138.

Rupke, N. A., and D. J. Stanley, 1974, Distinctive properties of turbiditic and hemipelagic mud layers in the Algéro-Balearic Basin, western Mediterranean Sea: Smithsonian Contributions to the Earth Sciences, no. 1, 40 p.

Sanders, J. E., 1965, Primary sedimentary structures formed by turbidity currents and related sedimentation mechanisms, *in* G. V. Middleton, ed., Primary sedimentary structures and their hydrodinamic interpretation. Society of Economic Paleontologists and Mineralogists, Special Publication 12, p. 192–219.

Sclater, J. G., and P. a. F. Christie, 1980, Continental stretching: An explanation of the post-Mid-Cretaceous subsidence of the Central North Sea Basin: Journal of Geophysical Research: Solid Earth, v. 85, no. B7, p. 3711–3739, DOI: 10.1029/JB085iB07p03711.

Schieber, J., 1998, Sedimentary features indicating erosion, condensation, and hiatuses in the Chattanooga Shale of Central Tennessee: Relevance for sedimentary and stratigraphic evolution, *in* J. Schieber, W. Zimmerle, and P. Sethi, eds., Mudstones and shales (vol. 1): Basin studies, sedimentology and paleontology: Stuttgart, Schweizerbart'sche Verlagsbuchhandlung, p. 187–215.

Schieber, J., 2003, Simple gifts and buried treasures-implications of finding bioturbation and erosion surfaces in black shales: The Sedimentary Record, v. 1, no. 2, p. 4–8.

Schieber, J., 2011, Reverse engineering mother nature—Shale sedimentology from an experimental perspective: Sedimentary Geology, v. 238, p. 1–22, DOI: 10.1016/j.sedgeo.2011.04.002.

Schieber, J., 2016, Mud-redistribution in epicontinental basins - Exploring likely processes: Marine and Petroleum Geology, v. 71, p. 119–133.

Schieber, J., and R. Bennett, 2013, Bedload transport of mud across a wide, storm-influenced ramp: Cenomanian–Turonian Kaskapau Formation, Western Canada foreland basin-discussion: Journal of Sedimentary Research, v. 83, no. 12, p. 1198–1199.

Schieber, J., and J. B. Southard, 2009, Bedload transport of mud by floccule ripples: Direct observation of ripple migration processes and their implications: Geology, v. 37, no. 6, p. 483–486.

Schieber, J., and Z. Yawar, 2009, A new twist on mud deposition: Mud ripples in experiment and rock record: The Sedimentary Record, v. 7, no. 2, p. 4–8.

Schieber, J., J. B. Southard, and K. G. Thaisen, 2007, Accretion of mudstone beds from migrating floccule ripples: Sciences, v. 318, no. 5857, p. 1760–1763.

Schieber, J., J. B. Southard, P. Kissling, B. Rossman, and R. Ginsburg, 2013, Experimental deposition of carbonate mud from moving suspensions: Importance of flocculation and implications for modern and ancient carbonate mud deposition: Journal of Sedimentary Research, v. 83, p. 1025–1031.

Schieber, J., J. B. Southard, and A. Schimmelmann, 2010, Lenticular shale fabrics resulting from intermittent erosion of water-rich muds: Interpreting the rock record in the light of recent flume experiments: Journal of Sedimentary Research, v. 80, no. 1, p. 119–128.

Soyinka, O. A., and R. M. Slatt, 2008, Identification and micro-stratigraphy of hyperpycnites and turbidites in Cretaceous Lewis Shale, Wyoming: Sedimentology, v. 55, no. 5, p. 1117–1133.

Spalletti, L. A., and G. D. Veiga, 2007, Variability of continental depositional systems during lowstand sedimentation: An example from the Kimmeridgian of the Neuquén Basin, Argentina: Latin American Journal of Sedimentology and Basin Analysis, v. 14, no. 2, p. 85–104.

Stetten, E., F. Baudin, J. L. Reyss, P. Martinez, K. Charlier, J. Schnyder, C. Rabouille, B. Dennielou, J. Coston-Guarini, and A. Pruski, 2015, Organic matter characterization and distribution in sediments of the terminal lobes of the Congo deep-sea fan: Evidence for the direct influence of the Congo River: Marine Geology, v. 369, p. 182–195.

Tesi, T., A. Asioli, D. Minisini, V. Maselli, G. Dalla Valle, F. Gamberi, L. Langone, et al., 2017, Large-scale response of the Eastern Mediterranean thermohaline circulation to African monsoon intensification during sapropel S1 formation: Quaternary Science Reviews, v. 159, p. 139–154.

Vail, P. R., R. M. Mitchum, and S. Thompson, 1977, Seismic stratigraphy and global changes of sea level, Part 4: Global cycles of relative changes of sea level, *in* C. E. Payton, ed., Seismic stratigraphy—Applications to hydrocarbon exploration, AAPG Memoir 36, p. 83–97.

Varela, R. A., D. Marchal, S. Cuervo, E. F. Lombardo, Y. S. Perl, D. E. Hryb, P. Pateti, and O. Nielsen, 2020, Geomechanics: Pressure, stress field, and hydraulic fractures, *in* D. Minisini, M. Fantín, I. Lanusse Noguera, and H. A. Leanza, eds., Integrated geology of unconventionals: The case of the Vaca Muerta play, Argentina: AAPG Memoir 121, p. 351–376.

Vittore, F., D. T. Licitra, L. Monti, I. Lanusse Noguera, C. Hernández, H. Reijenstein, and J. Quiroga, 2020, Full development phase of the Loma Campana block: Black oil to gas and condensate windows, *in* D. Minisini, M. Fantín, I. Lanusse Noguera, and H. A. Leanza, eds., Integrated geology of unconventionals: The case of the Vaca Muerta play, Argentina: AAPG Memoir 121, p. 417–444.

Weger, R. J., L. Rodriguez Blanco, and G. P. Eberli, 2017, A basinal reference section and lateral variability of the Vaca Muerta formation in the Neuquén Basin, Argentina, *in* 20° Congreso Geológico Argentino, 7–11 August, San Miguel de Tucumán, Argentina, p. 179–184.

Westphal, H., M. J. Head, and A. Munnecke, 2000, Differential diagenesis of rhythmic limestone alternations supported by palynological evidence: Journal of Sedimentary Research, v. 70, no. 3, p. 715–725.

Wilson, P. A., and H. H. Roberts, 1992, Carbonate-periplatform sedimentation by density flows: A mechanism for rapid off-bank and vertical transport of shallow-water fines: Geology, v. 20, p. 713–716.

Wilson, P. A., and H. H. Roberts, 1995, Density cascading: Off-shelf sediment transport, evidence and implications, Bahama Banks: Journal of Sedimentary Research, v. 65, p. 45–56.

Wilson, R., and J. Schieber, 2014, Muddy prodeltaic hyperpycnites in the Lower Genesee Group of Central New York, USA: Implications for mud transport in epicontinental seas: Journal of Sedimentary Research, v. 84, no. 10, p. 866–874.

Wilson, R., and J. Schieber, 2015, Sedimentary facies and depositional environment of the Middle Devonian Geneseo Formation of New York, USA: Journal of Sedimentary Research, v. 85, no. 11, p. 1393–1415.

Yawar, Z., and J. Schieber, 2017, On the origin of silt laminae in laminated shales: Sedimentary Geology, v. 360, p. 22–34, DOI: 10.1016/j.sedgeo.2017.09.001.

Zavala, C., and M. Arcuri, 2016, Intrabasinal and extrabasinal turbidites: Origin and distinctive characteristics: Sedimentary Geology, v. 337, p. 36–54.

Zavala, C., J. J. Ponce, M. Arcuri, D. Drittanti, H. Freije, and M. Asensio, 2006, Ancient lacustrine hyperpycnites: A depositional model from a case study in the Rayoso Formation (Cretaceous) of west-central Argentina: Journal of Sedimentary Research, v. 76, no. 1, p. 41–59.

Zeller, M., S. B. Reid, G. P. Eberli, R. J. Weger, and J. L. Massaferro, 2015a, Sequence architecture and heterogeneities of a field-scale Vaca Muerta analog (Neuquén Basin, Argentina) - From outcrop to synthetic seismic: Marine and Petroleum Geology, v. 66, p. 829–847.

Zeller, M., K. Verwer, G. P. Eberli, J. L. Massaferro, E. Schwarz, and L. Spalletti, 2015b, Depositional controls on mixed carbonate–siliciclastic cycles and sequences on gently inclined shelf profiles: Sedimentology, v. 62, p. 2009–2037.